Keitel *et al. Annals of Microbiology* (2024) 74:7
https://doi.org/10.1186/s13213-023-01745-4

Annals of Microbiology

UNIVERSITÀ DEGLI STUDI DI MILANO

ORIGINAL ARTICLE

Open Access

Process analysis of the anaerobe *Phocaeicola vulgatus* in a shake flasks and fermenter reveals pH and product inhibition

Laura Keitel[1†], Katharina Miebach[1†], Lea Rummel[1], Stanislav Yordanov[1] and Jochen Büchs[1*]

Abstract

Purpose The anaerobic gut bacterium *Phocaeicola vulgatus* (formerly *Bacteroides vulgatus*) has a significant role in the human gut microbiome. It can produce bioactive compounds with antimicrobial properties and industrially relevant organic acids like succinate. However, there is a knowledge gap in understanding the metabolism of *P. vulgatus*, as cultivation of anaerobic gut bacteria is challenging and usually conducted with enriched microbiota cultures. We aim to close this gap by characterizing this anaerobe bacterium in different cultivation conditions and scales.

Methods In this work, axenic cultures were studied in a shake flask and 2 L fermenter scale to characterize the influence of initial pH, buffer concentration, osmolality, and product inhibition on growth and organic acid production by *P. vulgatus*. Both cultivation systems had online gas measurements for total gas and CO_2 production. HPLC analysis generated closed carbon balances, accounting for all produced acids.

Results Total gas transfer rates and CO_2 transfer rates revealed that 65% of produced gas was attributed to H_2, while just 35% was connected to CO_2 production. A minimum buffer concentration of 50 mM MOPS and an initial pH of 7.3 were identified to mitigate pH inhibition in *P. vulgatus* cultivations with a defined minimal medium and glucose as substrate. The initial addition of lactate showed an inhibitory effect, starting at a concentration of 1 g L^{-1}. On the contrary, initial acetate addition was beneficial for organic acid production. A comparison of a pH-buffered and a pH-controlled 2 L fermentation demonstrated a switch in acid production toward succinate under pH control.

Conclusion The study provides insight into improved cultivation conditions for the gut bacterium *P. vulgatus* and demonstrates a successful scale-up from the shake flask to the 2 L bioreactor. By applying pH control in the bioreactor, growth was increased, and the organic acid production was switched from lactate to succinate. Even though *P. vulgatus* could serve as a production organism for interesting bioactive compounds and organic acids, further characterization and improvement are necessary to improve titers.

Keywords Anaerobic gut bacteria, *Phocaeicola (Bacteroides) vulgatus*, Cultivation medium restrictions, Product inhibition, Organic acids, AnaRAMOS, Online monitoring, Scale-up

Background

With circa 10^{7-14} organisms per milliliter of colonic contents, the gut microbiome is the largest share of bacteria in humans (Vos et al. 2022) and plays a crucial part in human health (Wilson et al. 2020). The phylum *Bacteroidota* dominates the human gut (Salyers 1984; Wexler 2007), achieves high yields of organic acids (Macfarlane and Macfarlane 2003; Ríos-Covián et al.

†Laura Keitel and Katharina Miebach contributed equally to this work.

*Correspondence:
Jochen Büchs
jochen.buechs@avt.rwth-aachen.de
[1] Chair of Biochemical Engineering (AVT.BioVT), RWTH Aachen University, Forckenbeckstraße 51, Aachen 52074, Germany

2016; Mayhew et al. 1975), and can be genetically modified (Lück and Deppenmeier 2022; Neff et al. 2023). Moreover, there is evidence that *Bacteroidota* can produce antibiotic or bioactive compounds (Brinkmann et al. 2022; Wexler 2007) and serve as probiotics (Tan et al. 2019). *Phocaeicola vulgatus*, a species of the phylum *Bacteroidota* and classified initially as *Bacteroides vulgatus* (García-López et al. 2019), is one of the most abundant and frequently isolated bacteria in human feces (Salyers 1984). *P. vulgatus* can degrade a variety of polysaccharides (Chung et al. 2017; Sonnenburg et al. 2010), making it a suitable candidate for sustainable antibiotic or bioactive compound, short-chain fatty acid (SCFA) production based on renewable materials or as a probiotic. Despite its potential to produce valuable materials, *P. vulgatus* has not yet been used in biotechnological processes (Lück and Deppenmeier 2022) since the strain has not been sufficiently characterized in axenic culture and for industrial processes. Strains of the phylum *Bacteroidota* were primarily characterized in the 1970s and 80s, but the focus was mainly on their pathological relevance (Cato and Johnson 1976; Macy and Probst 1979; McCarthy et al. 1988; Salyers 1984; Onderdonk et al. 1983). Cultivating anaerobic gut bacteria is complex due to the high degree of adaptation to the gastrointestinal ecosystem (Wexler 2007; Savage 1977). Thus, this study aims to profoundly characterize *P. vulgatus* in axenic culture and different cultivation conditions and scales for future applications. To our knowledge, no scientific work to date characterizes *P. vulgatus* in axenic culture and optimizes the process conditions.

One key aspect of characterizing *P. vulgatus* is its carbon metabolism. Reilly (1980) and Franke (2020) have shown that *P. vulgatus* requires CO_2 or bicarbonate supplementation for growth on agar plates and in the mineral medium. Related *Bacteroides* use one of the three glycolytic pathways to obtain products, such as acetate, propionate, succinate, lactate, formate, CO_2, and H_2 (Fischbach and Sonnenburg 2011), further explain that during anaerobic respiration, *Bacteroides* produce succinate by CO_2 fixation. The bacterium can regenerate CO_2 from succinate under CO_2-limiting conditions and produce propionate in the process. Furthermore, lactate is formed by reducing pyruvate via lactate dehydrogenase (Lück and Deppenmeier 2022). *Prevotella copri*, another *P. vulgatus*-related strain, is known to convert pyruvate to formate, CO_2, Fd_{red} (possible site for hydrogen formation), and acetyl-CoA (Franke and Deppenmeier 2018). The acetyl-CoA is then converted to acetate. Franke and Deppenmeier (2018) described the carbon metabolism and SCFA production of *P. copri*. They found a more pronounced CO_2 dependency of *P. copri* than *P. vulgatus*. The different CO_2 dependency leads to variations in the SCFA metabolism of both strains, as SCFA production partly relies on CO_2 (Fischbach and Sonnenburg 2011).

As previously stated, among the products of *P. vulgatus* are the SCFAs acetate, propionate, succinate, and formate, as well as lactate, a short-chain hydroxy fatty acid, denoted as SCFA in this study. These acids reach concentrations of 50–200 mM in the human intestine (Flint et al. 2012; Louis and Flint 2017; Koh et al. 2016; Cummings et al. 1987; Cummings and Macfarlane 1991) and are essential for gut bacteria to regulate the production of redox equivalents in the anaerobic environment of the intestine (van Hoek and Merks 2012). Besides their biological function, SCFAs are substrates in the chemical industry. Currently, most SCFAs are produced based on fossil raw materials with a high energy demand, even though, e.g., acetate and formate are part of the metabolism of various microbial species (Bulushev and Ross 2018; Lim et al. 2018). Only lactate is mainly produced biotechnologically by anaerobic bacteria (Ghaffar et al. 2014). One way of biologically producing SCFAs, which is still in its infancy, is using anaerobic sludge fermentation. The hereby produced SCFA yields and composition are depending on fermentation pH, temperature, and retention time (Wang et al. 2019). Hence, the characterization of the SCFA production by *P. vulgatus* can pave the way for a sustainable process optimally based on organic waste streams.

Only limited process characterization of *P. vulgatus* on larger scales has been conducted so far. In comparison, the scale-up of the *B. fragilis* for succinate production into a 10 L scale resulted in an increase of succinate production from 0.7 to 12.5 g L^{-1} (Isar et al. 2006) and a further increase to 20.0 g L^{-1} succinate using a statistical approach response surface methodology (Isar et al. 2007). More successful scale-ups were performed with enriched mixed cultures of anaerobic gut bacteria (Adamberg and Adamberg 2018; Adamberg et al. 2015), demonstrating that *Bacteroidota* have potential in process optimization and scale-up. Anaerobic mixed cultivation is a promising approach to improve production processes with *P. vulgatus* based on organic waste streams (Battista et al. 2022; Pau et al. 2022; Valentino et al. 2021). Kattel et al. (2023) have shown that a mixed culture benefits *P. vulgatus*. This is to be expected, as *P. vulgatus* naturally coexists in mixed culture in the gut. An enhanced growth rate and positive cross-feeding interactions were the findings of Kattel et al. (2023). After *P. vulgatus* has been characterized in axenic culture, mixed culture cultivations could be the next step to further increase growth and the production of valuable compounds and to utilize organic residual streams, e.g., from agriculture or food industries (Greses et al. 2022). A scale-up is a promising approach

to increase the production of valuable compounds produced by *P. vulgatus*. However, potential product inhibition by SCFA, like acetate, lactate, and succinate, could be challenging. Product inhibition of the model organism *E. coli* by acetate (Pinhal et al. 2019) and by acetate combined with other acids (Landwall und Holme 1977) is well-known and pH-dependent (Wolin 1969). Duncan et al. 2009 also showed that for *Bacteroides thetaiotaomicron*, inhibition of the organism by acids depends on the cultivation pH. Wang et al. 2020 demonstrated that several representatives of *Bacteroidetes* are sensitive to the accumulation of lactate and are inhibited even stronger by lactate in the presence of acetate.

This study aims to advance the characterization of *P. vulgatus* in terms of growth and optimized cultivation conditions. The characterization is performed on a small scale under anaerobic cultivation conditions and then proceeds to an initial scale-up to a 2 L stirred tank reactor. The influence of buffer, pH, osmolality, and initial acid concentration is investigated to identify optimal growth conditions and investigate possible inhibition factors. The study uses the Anaerobic Respiration Activity MOnitoring System (AnaRAMOS), a small-scale shaken cultivation system that allows non-invasive online measurement of CO_2 and pressure (Munch et al. 2020). This system determines the microbial gas transfer rate (Anderlei and Büchs 2001; Anderlei et al. 2004), at which gases, such as CO_2, are exchanged between the microorganisms and their surrounding environment. More precisely, the gas transfer rates applied in this work quantify the molar amount of gas produced by the microorganisms considering the liquid filling volume in the bioreactor and time in [mmol L^{-1} h^{-1}]. The AnaRAMOS is an alternative to traditional serum flasks that lack online measurement options and is thus applied for all parallelized characterization experiments of *P. vulgatus* in this study.

Material and methods

Strain and media

Phocaeicola vulgatus DSM 1447 was kindly provided by the research group of Prof. Deppenmeier from the Rheinische Friedrich-Wilhelms University, Bonn, and was obtained from the German Collection of Microorganisms and Cell Cultures (DSMZ, Brunswick, Germany). The culture was revived in Brain Heart Infusion medium (BHI) from BD Difco™ (Thermo Fisher, DE). When the BHI medium powder was solved in water, it contained 7.7 g L^{-1} calf brain, 9.8 g L^{-1} beef heart, 10 g L^{-1} protease peptone, 2 g L^{-1} dextrose, 5 g L^{-1} sodium chloride, and 2.5 g L^{-1} disodium phosphate. Cryogenic stocks were made from the active growing BHI culture after 24 h by mixing 50% v/v culture broth with 50% v/v anaerobic sucrose solution (500 g L^{-1}) and freezing 1.8 mL aliquots at − 80 °C.

The defined minimal medium with glucose (DMM-G) was used for all cultivations. The medium composition was based on Varel and Bryant (1974) and Lück and Deppenmeier (2022), with the deviation that MOPS buffer (3-(*N*-morpholino)propanesulfonic acid) was used instead of bicarbonate buffer. If not stated otherwise, the DMM-G medium components were purchased from Carl Roth (DE). The medium comprised 13 individual stock solutions, as some medium components were light- and temperature-sensitive, and premature mixing would have caused precipitation. The following stock solutions were prepared separately and mixed just before the experiments: Base components (pH 7.4), glucose, calcium chloride, magnesium chloride, iron(II)sulphate, SL6-trace elements, Wolin's vitamin solution (Koblitz et al. 2023), butyrate, vitamin K1, hemin, resazurin (Thermo Fisher, DE), L-cysteine hydrochloride, and MOPS buffer (pH 7.4). The base components stock solution was set to pH 7.4 with 5 M sodium hydroxide (NaOH) and comprised of ammonium chloride, dipotassium phosphate, monopotassium phosphate, and sodium chloride. The SL6-trace elements included boric acid, cobalt(II)chloride hexahydrate, copper(II)chloride dihydrate, manganese(II) chloride tetrahydrate (Merck, DE), nickel(II)chloride, sodium molybdate dihydrate, and zinc sulfate heptahydrate (Merck, DE). The Wolin vitamin stock solution contained α-lipoic acid, biotin, folate (Sigma Aldrich, DE), nicotinamide, p-aminobenzoic acid (Sigma Aldrich, DE), pantothenic acid (AppliChem, DE), pyridoxine hydrochloride (Sigma Aldrich, DE), riboflavin (Sigma Aldrich, DE), thiamine hydrochloride, and vitamin B12. The final concentrations of all components in the DMM-G medium are listed in Table S1. Base components, glucose, calcium chloride, magnesium chloride, iron(II)sulphate, and SL6-trace elements stocks were moist–heat sterilized at 121 °C for 20 min with a slow end-cooling phase to prevent liquid loss due to boiling. Heat-sensitive stock solutions were sterile-filtered with 0.22 µm polyethersulfone filters (Merck, DE). The reducing agent L-cysteine was sterile-filtered and stored in a serum bottle with an anaerobic nitrogen atmosphere to prevent premature oxidative reactions. After sterilization, Wolin's vitamin solution, vitamin K1, hemin, and resazurin stock solutions were stored light-protected at 4 °C. All other stock solutions were stored at room temperature.

Cultivation conditions and online analysis methods

Precultures of *P. vulgatus* were grown in 250 mL serum bottles. First, 50 or 150 mL of DMM-G medium was filled into the serum bottle. The bottle was sealed gas-tight with a rubber stopper and clamp and gassed with N_2 for 20 min to ensure anaerobic conditions. Then, CO_2 was transferred into the bottle with a sterile syringe to reach

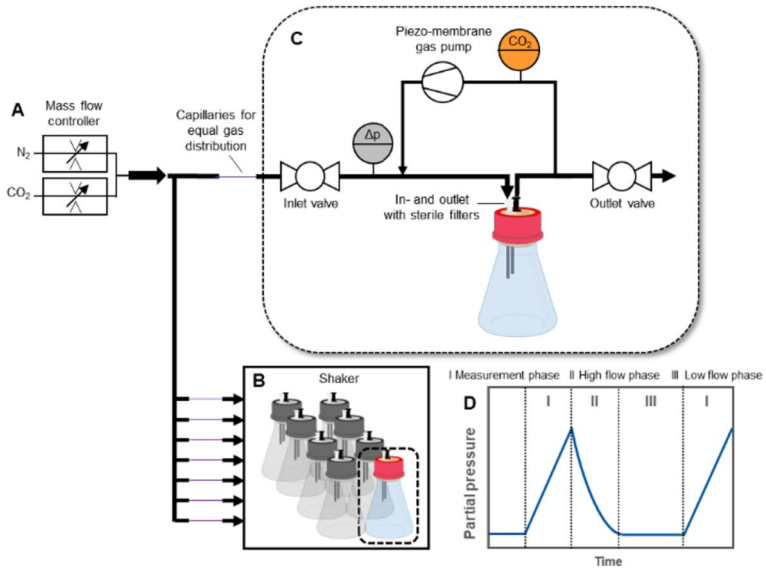

Fig. 1 Schematic overview of the AnaRAMOS setup and measurement principle. Based on Miebach et al. 2023. **A** Gas supply with mass flow controllers (MFC) and capillaries for even gas distribution to all eight flasks. **B** Temperature-controlled shaker containing eight shake flasks. **C** Measurement loop of one shake flask with in- and outlet valve, piezo-membrane gas pump, carbon dioxide sensor, and pressure sensor. **D** Gas transfer rate measurement principle based on cyclically repeated phases. Dotted lines and Roman numerals (I to III) represent phase changes. Phase I: 20 min measurement phase with closed valves, leading to gas accumulation and concentration increase in the headspace. Phase II: Valves open. 2.38 min high flow phase with increased gas flow (22.5 mL min^{-1}) of the cultivation gas through the headspace. Phase III: 40 min low flow phase with low gas flow (10 mL min^{-1}) in the flask headspace with cultivation gas

a headspace concentration of 10 Vol.-% CO_2. Before inoculation with 500 µL cryogenic culture, 0.1 or 0.3 mL of L-cysteine (2 M) as a reducing agent was injected into the 50 or 150 mL medium, respectively. Serum bottles were placed in a 37 °C temperature-controlled shaker with a shaking diameter of 50 mm and shaken at 100 rpm for 20–24 h.

All shake flask cultivations were performed as duplicates using the AnaRAMOS, designed by Munch et al. (2020). The AnaRAMOS setup is based on the RAMOS, originally established for aerobic cultivations (Anderlei and Büchs 2001; Anderlei et al. 2004). The AnaRAMOS enables non-invasive online measurement of total pressure and CO_2 under anaerobic conditions for up to eight shake flasks. A schematic overview of the setup is shown in Fig. 1.

It applies three cyclically repeated phases to obtain total gas transfer rates (TGTR) and carbon dioxide transfer rates (CTR). In the first phase, called the measurement phase, valves close each shake flask gastight, and microbially produced gases accumulate. The increase of the produced gases in the headspace of the flask over time is detected with pressure sensors (26PCA, Honeywell, USA) and infrared carbon dioxide sensors (MSH-P – CO2, 126 Dynament, UK). Compared to direct off-gas detection, the measurement phase with closed valves in the AnaRAMOS increases the measurement sensibility since gasses accumulate in the headspace. The gas transfer rates are then calculated by the following Eq. (1) and (2), adapted from Munch et al. (2020).

$$TGTR\left[\frac{mmol}{L \cdot h}\right] = \frac{n_{totalgas,m}}{V_L \cdot t_m} = \frac{\Delta p_{totalgas}}{\Delta t} \cdot \frac{V_G}{R \cdot T \cdot V_L} \quad (1)$$

$$CTR\left[\frac{mmol}{L \cdot h}\right] = \frac{n_{CO2,m}}{V_L \cdot t_m} = \frac{\Delta p_{CO2}}{\Delta t} \cdot \frac{V_G}{R \cdot T \cdot V_L} \quad (2)$$

Where n_m = moles of total gas or CO_2 formed in the measurement phase [mmol], V_L = liquid filling volume of the shake flask [L], t_m = duration of the measurement phase [h], Δp = change of total gas or CO_2 partial pressure in the measurement phase [bar], V_G = gas volume in the shake flask [L], R = standard gas constant [0.08314 bar L mol^{-1} K^{-1}], and T = temperature [K].

In the second phase of the AnaRAMOS, called the high-flow phase, cultivation gas is briefly purged through the flask headspace at an elevated flow rate to flush out produced gasses and quickly equilibrate the headspace with the desired cultivation gas of 1 Vol.-% CO_2 and 99 Vol.-% N_2. This phase is essential to minimize the possible influence of the accumulated gasses from the measurement phase. During the third phase, called the low-flow phase, each flask is gassed with the desired cultivation

gas at a low gas flow and for an extended time. Since the three phases must be adapted to the specific microorganism's metabolic activity, the time and gas flows per flask in this work differed from Munch et al. (2020). They were set to a 20-min measurement phase without gas flow, a 2.38-min high gas flow rate at 22.5 mL min^{-1}, and a 40-min low gas flow rate at 10 mL min^{-1}. Cultivations were continuously gassed during the high- and low-flow phases to avoid cross-influences of a changing gas composition when investigating other cultivation parameters, e.g., the initial pH. The shake flasks were filled with 45 mL sterile medium and then gassed overnight with the cultivation gas of 1 Vol.-% CO_2 and 99 Vol.-% N_2 to ensure anaerobic conditions. The shaker (ISF1-X, Adolf Kühner AG, DE) was set to a temperature of 37 °C and a shaking frequency of 100 rpm, with a shaking diameter of 50 mm. Before inoculation, the system was tested for gas tightness of each flask to ensure completely anaerobic conditions during cultivations. As a reducing agent, 0.1 mL L-cysteine was added to each flask by a sterile syringe through the gas-tight rubber stopper before inoculation with 5 mL preculture. Initial and final samples were drawn after inoculation and at the end of cultivation, respectively.

Bioreactor experiments were conducted in a double-wall glass bioreactor (Getinge Applikon, NL) with a total volume of 2.2 L and a filling volume of 1.5 L. A sufficient gas recirculation and consistent volume-specific gas flow (vvm) were chosen as scale-up parameters from shake flasks to the bioreactor. The gas recirculation was tested by slow-motion videos of gas bubbles in the filled bioreactor at 400, 500, and 600 min^{-1} stirring rates with two six-blade stirrers (Rushton turbine) installed at the same distance from each other, the reactor bottom, and the liquid surface. Screenshots of the slow-motion videos at 400 and 600 min^{-1} are provided in Supplement Fig. S1. Based on this test, a stirring rate of 600 min^{-1} was identified for complete gas recirculation. To evaluate the potential influence of shear stress on *P. vulgatus* at 600 min^{-1} in the bioreactor, the volume-specific power input was calculated for the applied shake flask and bioreactor cultivation conditions. Parameters and formulas for calculations are given in Supplement Table 2 and 3. A volume-specific power input of 0.034 kW/m^3 was calculated for shake flasks experiments, and 0.537 kW/m^3 was calculated for the bioreactor cultivation conditions. Typically, gas-sparged and stirred bioreactors have a volume-specific power input of around 1 kW/m^3 (Bredwell et al. 1999), while, for example, pressurized gas fermentations have a volume-specific power input < 0.3 kW/m^3 (Takors et al. 2018). The bioreactor conditions applied in this work with a volume-specific power input of 0.537 kW/m^3 were considered tolerable for *P. vulgatus*, and a biological scale-up comparison experiment was performed to confirm this assumption. The vvm in shake flasks was calculated by dividing 10 mL min^{-1} gas flow by 50 mL liquid medium, resulting in a vvm of 0.2 min^{-1}. Applied to the bioreactor, the gas flow had to be set at 300 mL min^{-1} when the filling volume was 1.5 L. The 300 mL min^{-1} gas was continuously supplied to the bioreactor to (i) maintain anoxic growth conditions for *P. vulgatus*, (ii) provide necessary CO_2 to the cultivation, and (iii) enable online gas analysis. The pH value of bioreactor cultivations was monitored continuously with an Easyferm plus PHI K8 200 (Hamilton, USA) probe. The exhaust gas was led through an X-Stream XEK analyzer (Emerson Electric Company, USA) with an infrared CO_2 sensor. Liquid samples were collected using a sterile sampling setup. Since the DMM-G medium is temperature sensitive, the medium and bioreactor were autoclaved independently at 121 °C for 20 min. The bioreactor was filled with water for sterilization. After sterilization, the water was drained from the bioreactor, and 1.35 L of sterile DMM-G medium was filled into the bioreactor. For pH-controlled cultivations, the buffer was omitted from the DMM-G medium. Instead, the pH was controlled at pH 7 using sterile NaOH (3 M). For pH-buffered cultivations, 50 mM MOPS buffer was included in the DMM-G medium, and pH control was deactivated. Before inoculation, the bioreactor was gassed for a minimum of 12 h with the cultivation gas of 1 Vol.-% CO_2 and 99 Vol.-% N_2 at a gas flow rate of 300 mL min^{-1}. Before inoculation, the bioreactor was heated to 37 °C, and 3 mL L-cysteine (2 M) was added as a reducing agent. To start the cultivation, the bioreactor was inoculated with 150 mL *P. vulgatus* preculture, grown in a serum bottle with DMM-G medium. To prevent foaming in the bioreactor, 0.5 mL sterile antifoam (Pluraflac® LF 1300, BASF SE, DE) was manually added through the septum after 6 h cultivation time. Experiments were ended after TGTR and CTR declined, indicating the termination of the growth phase and acid production. Afterwards, no biological activity occurs.

Offline analysis

Liquid samples of biological duplicates were centrifuged at 18,000 rpm for 5 min. The supernatant was used for High-performance liquid chromatography (HPLC), offline pH, and osmolality analysis. Non-centrifuged samples were used for optical density (OD_{600nm}) measurement. In the pH-controlled fermentation, the remaining cell pellet was used for cell dry weight (CDW) determination to generate an OD_{600nm}/CDW correlation (Fig. S2).

During ongoing experiments, sample supernatant was collected and stored at − 80 °C for later analysis. For HPLC, samples were then thawed, diluted 1:10 (bioreactor experiments) or 1:5 (shake flasks experiments) with DI water, and filtered with 0.2 µm cellulose acetate filters (Merck, DE). For measurement of glucose, acetate, succinate, lactate, propionate, and formate concentrations, the HPLC device (Dionex, USA) was equipped with an organic acid resin column of 300 × 8 mm dimensions (CS-chromatography, DE) and set to 60 °C. 5 mM H_2SO_4 at a flow rate of 0.8 mL min^{-1} was used as eluent. As HPLC detectors, a UV/VIS, and a refractive index detector (RID) were applied. For offline pH measurement, the sample supernatant was measured with a pH electrode (Mettler-Toledo, USA). Medium osmolality was analyzed with a freezing point Osmomat 3000 (Gonotec, DE). The OD_{600nm} was determined at 600 nm using a 20 Genesys spectrophotometer (Thermo Scientific, DE). Samples were diluted with 0.9 Vol.-% NaCl. For CDW determination during the pH-controlled fermentation, 2 mL of culture broth was filled in previously dried and weighted 2 mL safe lock tubes and centrifuged at 18,000 rpm for 5 min. The supernatant was removed, and the remaining cell pellet was dried at 80 °C. After cooling to room temperature in a desiccator, the tubes were weighed again, and the weight difference with and without the cell pellet was used to determine the CDW in g L^{-1}. By correlating OD_{600nm} and CDW of the pH-controlled fermentation (Fig. S2), the equation $CDW = 0.563 \cdot OD_{600nm}$ was derived and applied to calculate the CDW in all other experiments.

Gas samples were analyzed by a Trace GC Ultra gas chromatograph (Thermo Fisher, DE) to identify the gases produced by *P. vulgatus*. The gas chromatograph had a thermal conductivity and a flame ionization detector. Gas samples were drawn with a syringe from a closed serum bottle cultivation of *P. vulgatus*, grown in BHI medium for 24 h at 37 °C and 100 rpm.

Carbon balances

Carbon balances were calculated for all experiments with the following Eq. 3:

$$Carbon_{in\ X}\left[\frac{mmol}{L}\right] = \frac{Carbon\ molecules_{\ in\ X}[-]}{M_X\left[\frac{g}{mol}\right]} \cdot c_X\left[\frac{g}{L}\right] \cdot 1000 \tag{3}$$

Where X is the specific compound, c is the concentration [g L^{-1}], M_X is the molar mass of the specific compound [g mol^1], $carbon\ molecules_{in\ X}$ is the number of carbon molecules in the specific compound [-], and $carbon_{in\ X}$ is the volumetric molar carbon in the specific compound [mmol L^{-1}].

The compounds glucose, acetate, lactate, succinate, propionate, formate, CO_2, and biomass of every sample were considered. Concentrations of glucose, acetate, lactate, succinate, propionate, and formate were obtained by HPLC measurement. The molar carbon calculation of *P. vulgatus* cells was based on data for related *Prevotella copri* with a carbon content of 48.5% (Franke 2020). Molar carbon from CO_2 was calculated from the CO_2 transfer rate (CTR) integral based on Munch et al. (2020) by Eq. 4:

$$CO_2\left[\frac{mmol}{L}\right] = \int_0^t CTR dt \tag{4}$$

After calculating each compound's volumetric molar carbon [mmol L^{-1}], the values were summed up to obtain every sample's total volumetric molar carbon content. To get relative values for the compounds, their molar carbon value was divided by the total carbon of the same sample, as shown in Eq. 5:

$$Carbon_{Sample\ n}[\%] = \frac{Carbon_{in\ X,\ Sample\ n}\left[\frac{mmol}{L}\right]}{Total\ Carbon_{Sample\ n}\left[\frac{mmol}{L}\right]} \tag{5}$$

Where *sample n* is designated to a specific sample number in a specific experiment, $carbon_{in\ X,\ sample\ n}$ is the volumetric molar carbon of the specific compound in sample n [mmol L^{-1}], and $total\ carbon_{sample\ n}$ is the sum of all carbon in this sample n [mmol L^{-1}]. The first sample of each cultivation was defined as 100% molar carbon to evaluate the deviation in molar carbon of every sample during the cultivation.

Software

Graphics were created with OriginPro® version 2019, 2020, or 2021 from OriginLab Corporation (Massachusetts, USA).

Results

Reference cultivation

As a first step, a reference culture was analyzed to characterize *P. vulgatus* growth and acid production. Figure 2 shows the online gas transfer rates, offline pH value, OD600nm, osmolality, and HPLC analytics.

The total gas transfer rate (TGTR) in Fig. 2a shows a value of 1.4 mmol L^{-1} h^{-1} after 1 h of cultivation and peaks at 6.8 h with a value of 2.2 mmol L^{-1} h^{-1}. Hereafter, it decreases until it reaches a value close to 0 mmol L^{-1} h^{-1} at 13.8 h. The TGTR has a wide peak. The same wide curve progression is visible for the carbon dioxide transfer rate (CTR) in Fig. 2b, with a CTR maximum of 0.8 mmol L^{-1} h^{-1}. The CTR peak is significantly lower

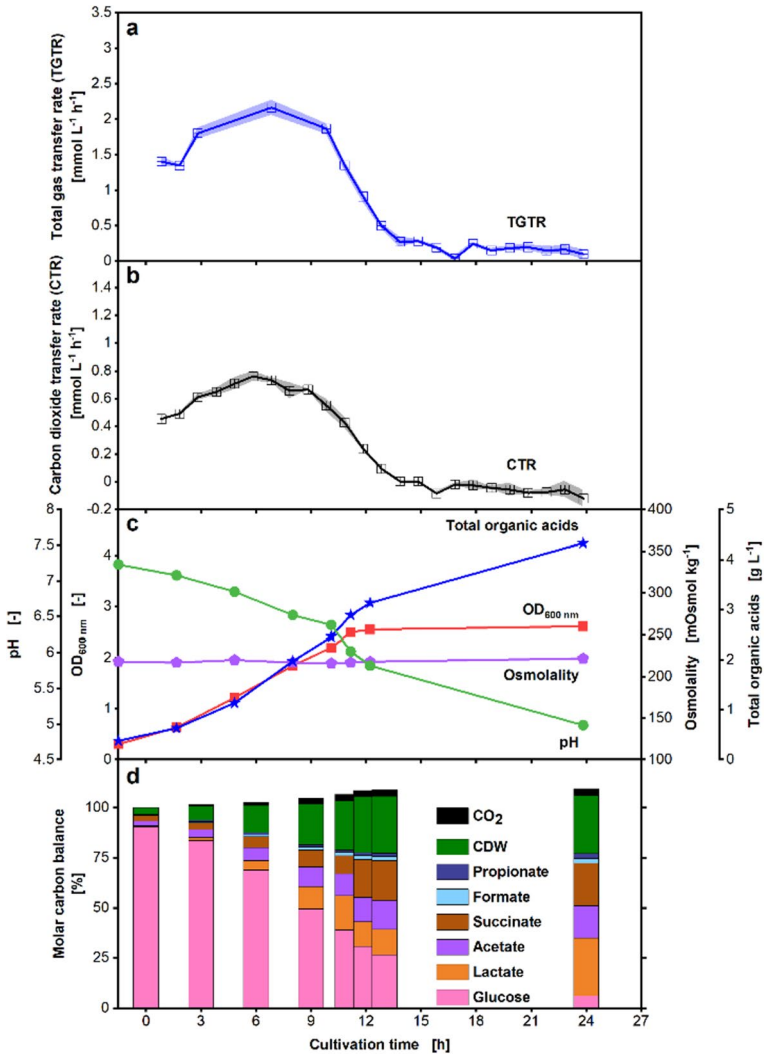

Fig. 2 Cultivation of *P. vulgatus* with online data and offline sampling in shake flasks. Online and offline profiles of a *P. vulgatus* cultivation in duplicates, Medium = DMMG, $c_{Glucose}$ = 6 g L^{-1}, c_{buffer} = 50 mM MOPS, T = 37 °C, n = 100 rpm, V_L = 50 mL, initial OD = 0.3, initial pH after inoculation = 7.23, vvm = 0.2 $min.^{-1}$, gas mix = 1% CO_2 and 99% N_2. **a** Total gas transfer rate (TGTR) and **b** carbon dioxide transfer rate (CTR), shadows indicate maximum and minimum values of duplicates (error bars). Offline data was obtained from the fermentation. **c** OD_{600nm}, pH, osmolality, and total organic acids as mean values of biological duplicates. **d** Molar carbon balance in % of initial total carbon, calculated with Eqs. 3–5

than the TGTR peak. CO_2 only contributes about 35% to the total gas.

In Fig. 2c, the offline analytics of the cultivation are shown. The pH (green circles) decreases throughout the cultivation, with a particularly strong decrease after 11 h. The final pH reaches a value of 5.0, and biomass production stops at 12 h at an OD_{600nm} (red squares) of 2.5. The osmolality (purple pentagons) remains constant during the cultivation at around 220 mOsmol kg^{-1}. HPLC measurement was performed for the key metabolites propionate, formate, succinate, acetate, and lactate (total organic acids, blue stars). Total organic acids increase during the whole course of the cultivation, even after 12 h, when the biomass production stops. A total of 4.3 g L^{-1} acids is reached. The molar carbon balance (Fig. 2d, calculated according to Eqs. 3–5) is closed with a maximum deviation of 9.1%, and the biomass accounts for 29% of the total carbon at the experiment's end. Little CO_2 is formed, reaching a maximum of 3.3% of the total carbon. However, as *P. vulgatus* produces and consumes CO_2, the CO_2 fraction of the total carbon must be regarded as a cumulative value. In the first 6 h of the cultivation, acetate and succinate are the most produced acids. After 9 h, lactate production increases strongly. Overall, little propionate

and formate are produced, and a small amount of glucose is still present. Growth inhibition of *P. vulgatus* is visible in the data of OD_{600nm} and by the fact that glucose is still present at the end of the cultivation. Therefore, the next step was to test possible cultivation parameters that could lead to inhibition. These parameters were the buffer concentration, the initial osmolality, the initial pH, and the addition of the acids formed by *P. vulgatus*. The buffer concentration was chosen to prevent pH inhibition. As higher buffer concentrations also increase the osmolality, higher initial osmolalities were tested to exclude negative effects caused by the high osmolalities of high buffer concentrations. Higher initial pH values were examined to obtain a higher pH value during the cultivation and prevent pH inhibition. The influence of the produced acids lactate, acetate, and succinate was also examined, as they might be another cause for inhibition.

Characterization of cultivation process conditions

The buffer concentration was varied as a next step to distinguish the process. During the experiment shown in Fig. 3, media with concentrations ranging from 0 to 150 mM MOPS were tested.

Figure 3a shows that the TGTR for a MOPS concentration of 0 mM (red circles) has a distinct peak. Compared to the TGTR peaks of other MOPS concentrations, there is a decreasing TGTR peak with increasing MOPS concentrations. The TGTR curves for 100 and 150 mM MOPS (green triangles and blue pentagons) are comparable. It is observed that higher MOPS concentrations prolong the production of gasses. The same trends can be seen for the CTR (Fig. 3b). Thus, the total CO_2 production throughout the cultivation remains constant for all MOPS concentrations. Comparing the TGTR and CTR peaks, a notable difference between 0 and 50 mM MOPS (red circles and black squares) can be seen. Differences between the CTR peaks of these conditions are higher than those of the TGTR peaks, and only the gas transfer rates for 0 mM MOPS show a distinct peak.

In Fig. 3c, the total organic acids increase with increasing MOPS concentration until a buffer concentration of 100 mM and stagnate hereafter. The total organic acid production doubled by increasing the buffer concentration from 0 to 50 mM MOPS. Formate is only produced with MOPS concentrations of 50 mM or higher. The proportions observed for propionate, succinate, and acetate production do not indicate a dependence on the MOPS concentration. However, lactate production increases with increasing MOPS concentrations until 100 mM MOPS. Overall, propionate and formate production is low compared to the other acids. The residual glucose is 2.9 g L^{-1} for 0 mM MOPS, 0.8 g L^{-1} for 50 mM MOPS, and 0 g L^{-1} for 100 and 150 mM MOPS. The final pH

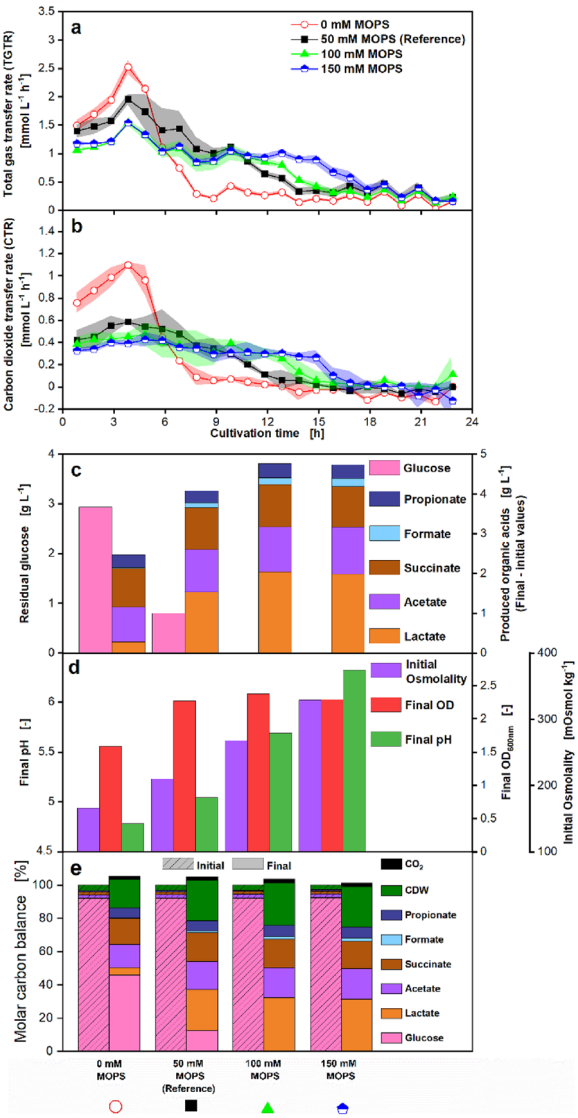

Fig. 3 Effect of different MOPS concentrations on *P. vulgatus* shake flask cultivations in duplicates. Medium = DMMG, $c_{Glucose}$ = 6 g L^{-1}, MOPS buffer (0, 50, 100, 150 mM), T = 37 °C, n = 100 rpm, V_L = 50 mL, initial OD = 0.3, initial pH after inoculation = 6.95–7.14, vvm = 0.2 min^{-1}, gas mix = 1% CO_2 and 99% N_2. **a** Online data of total gas transfer rate (TGTR) and **b** carbon dioxide transfer rate (CTR). Shadows indicate maximum and minimum values of duplicates (error bars). **c** Offline data of produced organic acids including propionate, formate, succinate, acetate, and lactate and remaining glucose; **d** initial osmolality, final OD_{600nm}, and final pH as mean values of biological duplicates. Samples to measure initial osmolality were drawn immediately after inoculation. Samples to measure final OD_{600nm}, final pH, and HPLC analysis were drawn immediately after termination of the experiment, indicated by the last online data point in **a** and **b**. **e** Molar carbon balance in % of the initial carbon, calculated with Eqs. 3-5. Initial values include acids from preculture

increases with increasing MOPS concentrations from 4.8 to 6.3, as shown in Fig. 3d. The final OD_{600nm} increases from 0 to 50 mM MOPS and reaches about the same values between 50 and 150 mM MOPS. The initial osmolality increases with increasing MOPS concentrations. The molar carbon balance is closed with a maximum deviation of 5.7% (Fig. 3e). Figure 3e supports the results from Fig. 3c and 3d and shows that the carbon flow goes toward lactate with increased MOPS concentration. Even though a MOPS concentration of 100 mM leads to higher organic acid concentrations, 50 mM MOPS was used for the following experiments, as the same final OD_{600nm} was reached, and the gas transfer rates were more distinct with 50 mM MOPS. The more pronounced online gas signal facilitates the interpretation of the other cultivation parameters. For future applications, when additional information about the gas transfer rates is not necessary, the authors would recommend using a MOPS concentration of 100 mM.

Figure 4 presents the effect of increasing osmolality on *P. vulgatus* growth and metabolic activity. The NaCl concentration in the medium was varied to achieve different osmolality levels.

The TGTR (Fig. 4a) of the reference osmolality, 220 mOsmol kg^{-1} (no added NaCl, black squares), reaches the highest maximum of 1.9 mmol L^{-1} h^{-1} with a plateau over 4 h. Higher osmolality levels significantly lower the TGTR and CTR maximum (Fig. 4b) and simultaneously extend the gas production. The CTR of the reference osmolality also shows the highest maximum but without the plateau of the TGTR. Figure 4c shows that organic acid production decreases with an increasing osmolality level. Hereof, succinate and acetate show a slight decrease with increasing osmolalities, and lactate increases with increasing osmolality. Formate is not detected in this experiment. Glucose is never fully consumed under the investigated conditions, while residual glucose concentrations increase with increasing osmolality levels. The final pH (Fig. 4d) increases from 4.8 to 5.2 with increasing osmolality. The final OD_{600nm} increases from 1.7 to 2.2 with increasing osmolality, except for 301 mOsmol kg^{-1}, where the final OD_{600nm} is 1.5 and, therefore, lower than the final OD_{600nm} for 220 mOsmol kg^{-1} and 349 mOsmol kg^{-1}. Initial osmolalities are shown in Fig. 4d and have been measured after inoculation. The carbon balance (Fig. 4e) is closed for all cultivations with a maximum deviation of 5.4%. Figure 4e supports the results from Fig. 4c and 4d and clearly shows, as in Fig. 3, that with increased osmolality, the carbon flow goes toward lactate.

In the experiment displayed in Fig. 5, the influence of the initial pH value on the growth and acid production

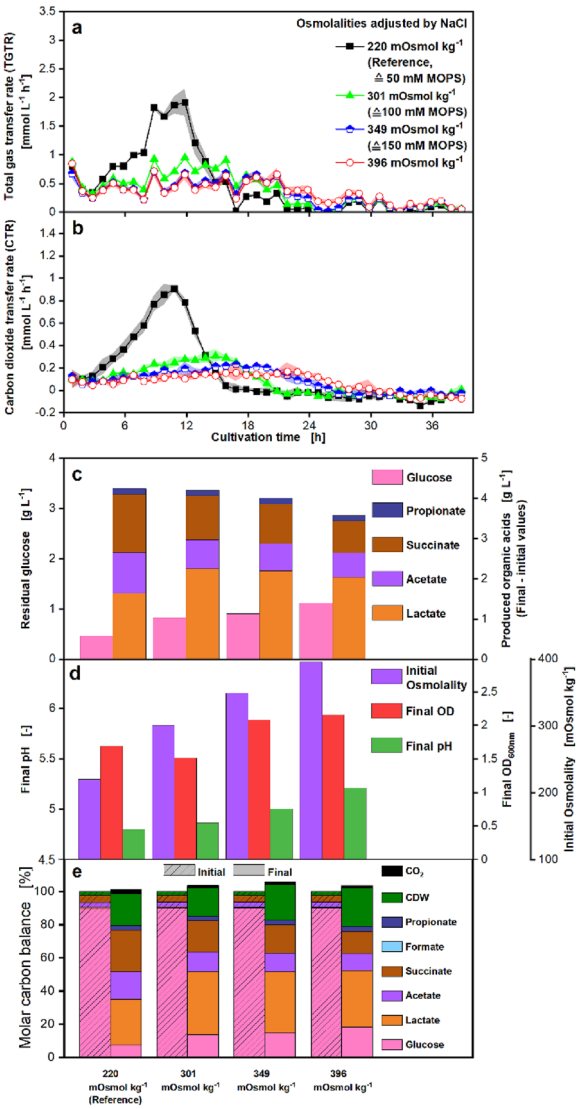

Fig. 4 Effect of different osmolalities on *P. vulgatus* shake flask cultivations in duplicates. Medium = DMMG, $c_{Glucose}$ = 6 g L^{-1}, c_{buffer} = 50 mM MOPS, T = 37 °C, n = 100 rpm, V_L = 50 mL, initial OD = 0.21, initial pH after inoculation = 7.03–7.08, vvm = 0.2 min^{-1}, gas mix = 1% CO_2, and 99% N_2, 220 mOsmol kg^{-1} as reference osmolality, osmolalities of 301, 349, and 396 mOsmol kg^{-1} adjusted by addition of NaCl. Online data of **a** total gas transfer rate (TGTR) and **b** carbon dioxide transfer rate (CTR), shadows indicate maximum and minimum values of duplicates (error bars). Offline data of **c** produced organic acids including propionate, succinate, acetate and lactate, and remaining glucose; **d** initial osmolality, final OD_{600nm}, and final pH as mean values of biological duplicates. Samples to measure initial osmolality were drawn immediately after inoculation. Samples to measure final OD_{600nm}, final pH, and HPLC analysis were drawn immediately after termination of the experiment, indicated by the last online data point in **a** and **b**. **e** Molar carbon balance in % of the initial carbon, calculated with Eqs. 3-5. Initial values include acids from preculture

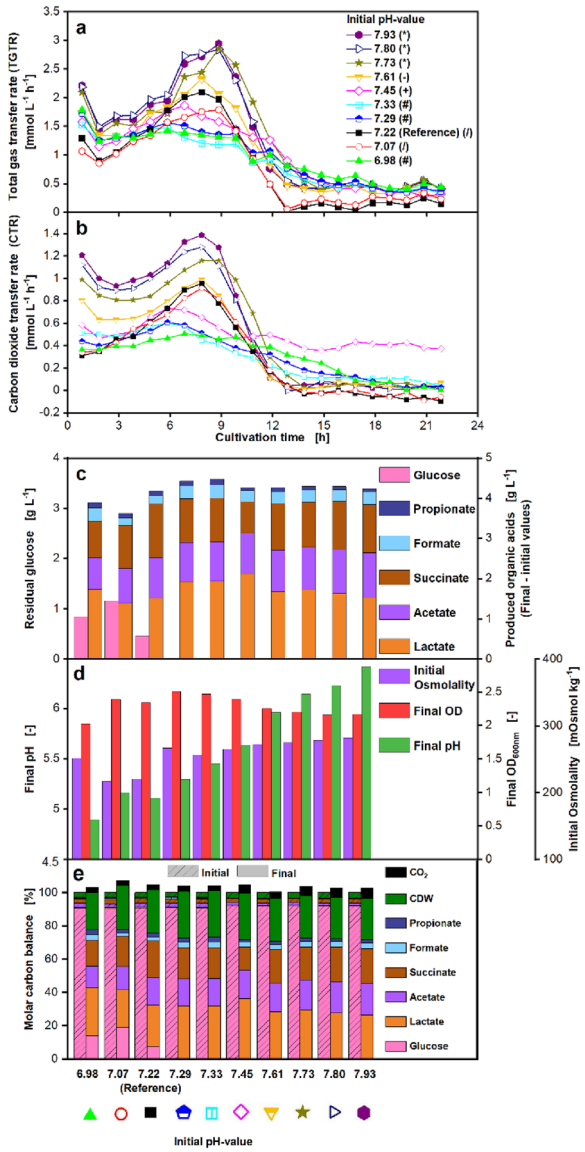

Fig. 5 Effect of changing the initial pH-value on *P. vulgatus* shake flask cultivations in duplicates. Medium = DMMG, $c_{Glucose}$ = 6 g L^{-1}, c_{buffer} = 50 mM MOPS, *T* = 37 °C, *n* = 100 rpm, V_L = 50 mL, initial OD = 0.3, different initial pH, vvm = 0.2 $min.^{-1}$, gas mix = 1% CO_2 and 99% N_2, tested initial pH values after inoculation: 6.98, 7.07, 7.22, 7.29, 7.33, 7.45, 7.61, 7.73, 7.80, and 7.93. **a** Online data of total gas transfer rate (TGTR) and **b** carbon dioxide transfer rate (CTR). Symbols in brackets indicate different experiments. **c** Offline data of produced organic acids including propionate, formate, succinate, acetate, and lactate and remaining glucose, **d** initial osmolality, final OD_{600nm}, and final pH as mean values of biological duplicates. Samples to measure initial osmolality were drawn immediately after inoculation. Samples to measure final OD_{600nm}, final pH, and HPLC analysis were drawn immediately after termination of the experiment, indicated by the last online data point in **a** and **b**. **e** Molar carbon balance in % of the initial carbon, calculated with Eqs. 3-5. Initial values include acids from preculture. The corresponding maximum and minimum of duplicates (error bars) can be found in Supplementary Fig. S3

of *P. vulgatus*, with initial pH values ranging from 6.98 to 7.93, was determined.

The TGTR curves (Fig. 5a) of the different initial pH values show significant differences after 1 h. The highest TGTR maximum was reached with an initial pH value of 7.93 (purple hexagons). The TGTR maximum decreases with decreasing initial pH, except in the pH range between 7.29 and 7.45, which does not follow this trend. Only for the higher initial pH values does the TGTR show a distinct peak. For the CTR (Fig. 5b), the same trends as for the TGTR are visible, with higher initial deviations for varying pH values. The corresponding maximum and minimum of TGTR and CTR duplicates are presented in Fig. S3a and b.

Figure 5c shows that acetate and formate production does not change for different initial pH values. Succinate production is highest with an initial pH of 7.22 and lactate production with an initial pH of 7.45. Propionate production is higher for initial pH values below 7.45. However, no strong trend concerning the initial pH's influence on each acid's production is visible. The highest total organic acid production is reached, with an initial pH of 7.33. Glucose is not fully consumed for initial pH values between 6.98 and 7.22. The final pH (Fig. 5d) increases with increasing initial pH. The OD_{600nm} is highest for an initial pH of 7.29 and 7.33. The initial osmolality is lowest for the reference cultivation with an initial pH of 7.22. The carbon balance (Fig. 5e) is closed with a maximum deviation of 7.3%. Figure 5e supports the results of Fig. 5c and 5d and shows that the carbon flux also moves toward different acids as the initial pH changes.

Influence of initial acid addition

As the main products of *P. vulgatus* are acids, an experiment was conducted to distinguish between the effects of pH and product inhibition. To do so, increasing concentrations of the main produced acids: lactate (Fig. 6), acetate (Fig. 7), succinate (Fig. S6 and Fig. S7), and mixtures thereof (Fig. S8-S10) were added to the medium, while the initial pH was set to 7.2 in all cultivations.

In Fig. 6a, no difference in the TGTR is visible between the reference (black squares) and the cultivation with 1.0 g L^{-1} lactate (red circles). However, the TGTR maximum decreases with increasing lactate addition. After 10 h cultivation, the progression of all TGTR curves, including the reference, is identical. A similar progression can be observed for the CTR, as displayed in Fig. 6b. Contrary to the TGTR, a lower CTR is already visible at a concentration of 1.0 g L^{-1} lactate compared to the reference. The CTR during the first 10 h decreases with increasing lactate addition, and CTR peaks can barely be identified. After 10 h cultivation time, the CTR curves align again. Comparing the reference and the cultivation

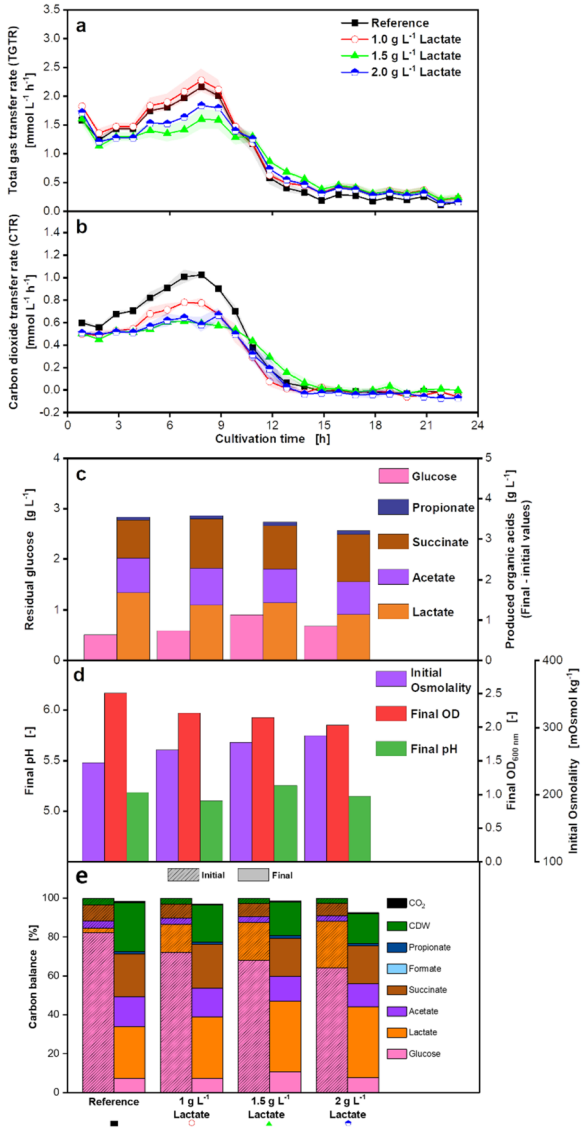

Fig. 6 Effect of initial lactate addition to *P. vulgatus* shake flask cultivations in duplicates. Medium = DMMG, $c_{Glucose}$ = 6 g L^{-1}, c_{buffer} = 50 mM MOPS, *T* = 37 °C, *n* = 100 rpm, V_L = 50 mL, initial OD = 0.35, initial pH after inoculation = 7.23, vvm = 0.2 min^{-1}, gas mix = 1% CO_2 and 99% N_2. Online data of **a** total gas transfer rate (TGTR) and **b** carbon dioxide transfer rate (CTR) shadows indicate maximum and minimum values of duplicates (error bars). Offline data of **c** produced organic acids including propionate, succinate, acetate and lactate, and remaining glucose; **d** initial osmolality, final OD_{600nm}, and final pH as mean values of biological duplicates. Samples to measure initial osmolality were drawn immediately after inoculation. Samples to measure final OD_{600nm}, final pH, and HPLC analysis were drawn immediately after termination of the experiment, indicated by the last online data point in **a** and **b**. **e** Molar carbon balance in % of the initial carbon, calculated with Eqs. 3-5. Initial values include acids from preculture. The corresponding molar carbon balance in $mmol_C$ $L.^{-1}$ can be found in Supplementary Fig. S4

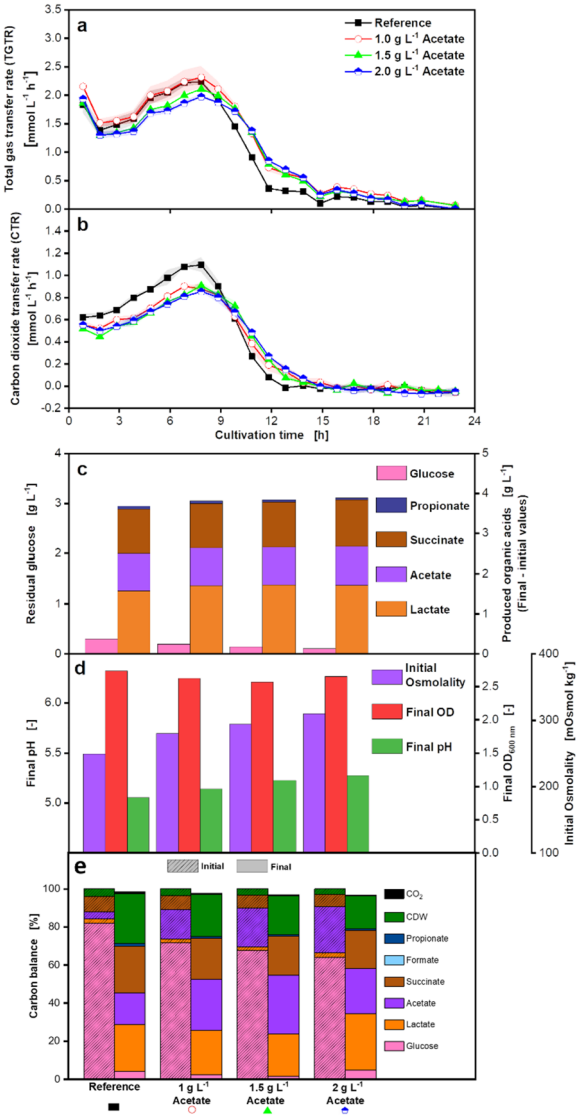

Fig. 7 Effect of initial acetate addition to *P. vulgatus* shake flask cultivations in duplicates. Medium = DMMG, $c_{Glucose}$ = 6 g L^{-1}, c_{buffer} = 50 mM MOPS, *T* = 37 °C, *n* = 100 rpm, V_L = 50 mL, initial OD = 0.40, initial pH after inoculation = 7.20, vvm = 0.2 min^{-1}, gas mix = 1% CO_2 and 99% N_2. Online data of **a** total gas transfer rate (TGTR) and **b** carbon dioxide transfer rate (CTR), shadows indicate maximum and minimum values of duplicates (error bars). Offline data of **c** produced organic acids including propionate, succinate, acetate and lactate, and remaining glucose; **d** initial osmolality, final OD_{600nm}, and final pH as mean values of biological duplicates. Samples to measure initial osmolality were drawn immediately after inoculation. Samples to measure final OD_{600nm}, final pH, and HPLC analysis were drawn immediately after termination of the experiment, indicated by the last online data point in **a** and **b**. **e** Molar carbon balance in % of the initial carbon, calculated with Eqs. 3-5. Initial values include acids from preculture. The corresponding molar carbon balance in $mmol_C$ $L.^{-1}$ can be found in Supplementary Fig. S5

with 1.0 g L^{-1} lactate addition in Fig. 6c, the total acid production is the same, but less succinate and more lactate are produced in the reference. For cultivations with the addition of 1.5 g L^{-1} lactate (green triangle) and 2.0 g L^{-1} lactate, the total acid production decreases slightly from 3.5 to 3.2 g L^{-1}. Less lactate is produced in cultivations with lactate addition compared to the reference. No production of the acid formate was detected in this experiment. The final OD_{600nm} in Fig. 6d declines from 2.5 to 2.0 with increasing lactate addition, while the final pH varies around 5.2 in all cultures. The initial osmolality values are higher with lactate addition and reach 290 mOsmol kg^{-1} with the addition of 2.0 g L^{-1} lactate. Glucose is still available at the end of all cultures and concentrations range from 0.5 to 0.9 g L^{-1}. Figure 6e confirms that the percentage of lactate in the produced acids further increased with increasing initial lactate addition.

In Fig. 7a, the TGTR maximum slightly decreases with 1.5 g L^{-1} (green triangle) and 2.0 g L^{-1} acetate addition (blue pentagon). Furthermore, the TGTR drop is less sharp in all cultures with acetate addition. As shown in Fig. 7b, all cultures with acetate addition show a lower CTR peak than the reference (black squares). Moreover, the CO_2 production of cultures with acetate addition occurs later and lower than in the reference. The production of acids, shown in Fig. 7c, increases with acetate addition. However, the ratio of produced acids remains constant at 1.8:1:1.2 for lactate to acetate to succinate. The acid formate is not detected in this experiment. The final OD_{600nm} in Fig. 7d is around 2.7, without a clear trend for cultivations with or without acetate addition. In contrast, Fig. 6e shows a decreasing percentage of the biomass (CDW) in the final carbon balance with increasing acetate addition. The final pH increases with increasing acetate addition, ranging from 5.0 to 5.3. The initial osmolality is higher with increasing acetate addition and reaches the highest initial value of 310 mOsmol kg^{-1} with 2.0 g L^{-1} acetate addition. Glucose is still available in all cultures, but the residual glucose decreases with increasing initial acetate addition. In the culture with 2.0 g L^{-1} acetate, the residual glucose concentration is detected at 0.1 g L^{-1}.

Succinate addition (Fig. S6 and Fig. S7) to DMM-G medium slightly increased the OD_{600nm}, while increasing concentrations of the acid mixtures led to decreasing OD_{600nm}, organic acid, and CO_2 formation (Fig. S8-S10).

Scale-up from shake flask to 2 L fermenter and effect of pH control

Cultivation with pH control is necessary to distinguish the possible effects of acid production and the associated pH reduction on cultivation behavior. Since pH control is best implemented in benchtop fermenters, a scale-up from the shake flask to the 2 L fermenter scale was conducted with a pH-buffered DMM-G medium (Fig. 8).

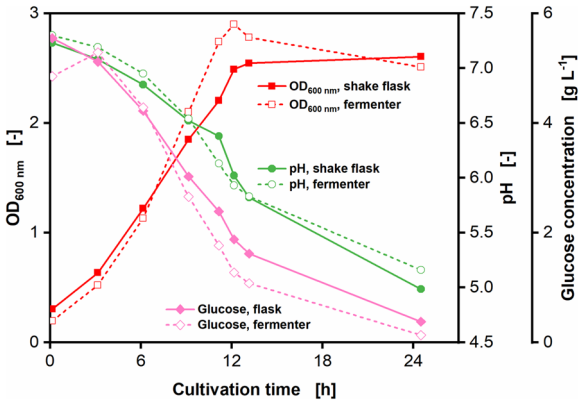

Fig. 8 Comparison of *P. vulgatus* cultivations in shake flask in duplicates and benchtop bioreactor. Offline samples OD_{600nm} (red squares), pH (green circles), and glucose (pink diamonds) of shake flask (filled symbols) and bioreactor cultivations (open symbols). Medium = DMMG, $c_{Glucose}$ = 6 g L^{-1}, c_{buffer} = 50 mM MOPS, T = 37 °C, $n_{fermenter}$ = 600 rpm, $n_{shake\ flask}$ = 100 rpm, $V_{L,fermenter}$ = 1500 mL, $V_{L,shake\ flask}$ = 50 mL, vvm = 0.2 min^{-1}, gas mix = 1% CO_2 in 99% N_2. After 6 h, 0.5 mL antifoam was added to the fermenter

The increase of the OD_{600nm} (red squares) and decrease of pH (green circles) and glucose concentration (pink diamonds) align in the shake flask and fermenter until 6 h cultivation time. Subsequently, a strong increase of OD_{600nm} to a maximum value of 2.9 is shown in the fermenter, while the shake flask reaches a maximum OD_{600nm} of 2.6. The OD_{600nm} increases linearly between 6 and 12 h in both cultivation scales. Corresponding to the higher final OD_{600nm}, glucose is consumed faster in the fermenter, and the final glucose concentration is at a very low concentration of 0.1 g L^{-1}. The final glucose concentration in the shake flask is 0.4 g L^{-1}. The pH shows the same course for both scales, except the final pH in the shake flask is 0.2 lower than in the fermenter.

After comparing the shake flask and 2 L fermenter with pH-buffered medium, a pH-controlled fermentation was conducted at pH 7.0. The results are displayed in Fig. 9 compared to the 2 L fermenter cultivation with a pH-buffered medium.

The fermenter with pH control shows an overall higher CTR (black lines), also in later cultivation phases after 12 h. The osmolality (purple pentagons) is lower in the non-buffered fermentation and starts at 152 mOsmol kg^{-1}, compared to 216 mOsmol kg^{-1} in the buffered fermentation. During the cultivation, the osmolality of the medium increases in the pH-controlled fermentation until both fermentations reach final values of 203–219 mOsmol kg^{-1}. The OD_{600nm} (red squares, Fig. 9b) increases comparably during the

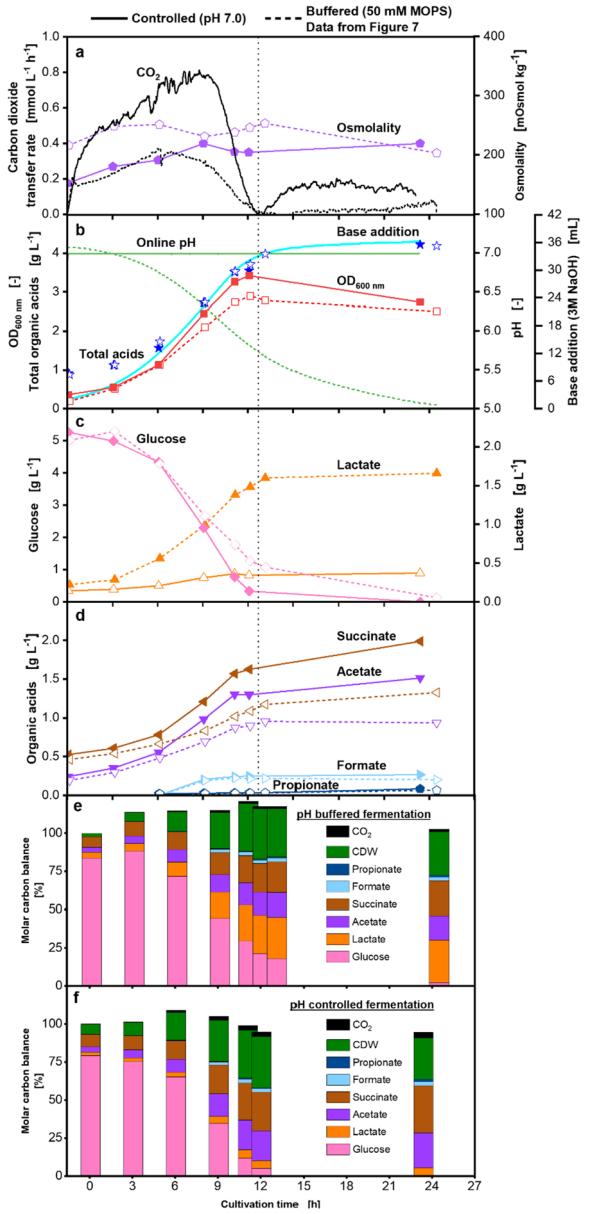

Fig. 9 Influence of pH control versus pH buffer on *P. vulgatus* in benchtop fermenter cultivations. Online and offline profiles of *P. vulgatus* cultivations with pH control at pH 7.0 (solid lines and filled symbols) or with 50 mM MOPS buffer (dashed lines and blank symbols, data from Fig. 8). Medium = DMMG, $c_{Glucose}$ = 6 g L^{-1}, T = 37 °C, n = 600 rpm, V_L = 1500 mL, vvm = 0.2 min^{-1}, gas mix = 1% CO_2, and 99% N_2. After 6 h, 0.5 mL of antifoam was added to the bioreactors. Online and offline data of **a** carbon dioxide transfer rate (CTR) and osmolality; **b** online pH (green lines), $OD_{600\ nm}$ (red squares), total acids (blue stars), and base consumption (turquoise line); **c** glucose (pink diamonds) and lactate (orange triangles) concentrations; **d** succinate (brown triangles), acetate (purple triangles), formate (light blue triangles), and propionate (dark blue pentagons) concentrations. The vertical dotted line refer to the pH-controlled fermentation and marks the time of the glucose depletion. **e–f** Molar carbon balance in % of the initial carbon, calculated with Eqs. 3-5. Initial values include acids from preculture

first 6 h in both fermentations. Then, the OD_{600nm} in the pH-controlled fermenter rises to a maximum value of 3.4, compared to the maximum OD_{600nm} of 2.9 in the buffered fermentation. The pH (green line) in the pH-controlled fermentation is maintained at pH 7.0. In comparison, the pH in the buffered fermentation decreases from pH 7.1 to pH 5.0 over 25 h cultivation time. The total acid (blue stars) production is identical in both fermentations and reaches 4.2 g L^{-1}. In the pH-controlled fermentation, the trend of the base consumption (turquoise line) is equivalent to the acid production and results in a total of 36 mL 3 M NaOH used to maintain the set pH 7.0. Glucose consumption (pink diamonds, Fig. 9c) is comparable until a cultivation time of 6 h. Afterward, glucose is consumed faster in the fermentation with pH control and depleted after approximately 13 h (vertical dotted line). A glucose concentration of 0.1 g L-1 is measured after 25 h in the pH-buffered fermentation. The individual acids are produced at different ratios in the pH-controlled and buffered fermentation. During the first 6 h, succinate (brown triangles) and acetate (purple triangles) are produced at the same rate in both fermentations, whereas lactate (orange triangles) production is higher in the pH-buffered fermentation. After 6 h, the acetate and succinate production rates in the pH-controlled fermentation exceed those in the pH-buffered fermentation. Lactate is the main acid produced in the pH-buffered fermentation with a final concentration of 1.7 g L^{-1}, while in the pH control fermentation, lactate concentrations are below 0.4 g L^{-1}. In comparison, the succinate concentrations reach 1.3 g L^{-} or 2.0 g L^{-1}, and acetate concentrations reach 0.9 g L^{-1} or 1.5 g L (light blue[1] in the pH-buffered and pH control fermentation, respectively. Formate (light blue triangles) and propionate (dark blue pentagons) production start after 6 h in both fermentations and concentrations reach maxima of 0.25 g L^{1} formate and 0.1 g L^{-1} propionate. The carbon balances in Fig. 9e–f confirm the switch in acid production.

Discussion

Reference cultivation

P. vulgatus' maximum total gas transfer rate of 2.2 mmol L^{-1} h^{-1} is very low compared to other gas-producing anaerobes like, for example, *C. pasteurianum*, with more than 20 mmol L^{-1} h^{-1} (Miebach et al. 2023). This is also illustrated in the pressure raw data for the reference cultivation, presented in Supplement Fig. S11. Nevertheless, the significantly higher TGTR than CTR (Fig. 2) suggests that, besides CO_2, other gases were produced. A gas chromatography measurement (data not shown) confirmed the H_2 production for *P. vulgatus*, as already

stated in earlier studies (Traore et al. 2019; Kazimierowicz et al. 2022; McKay et al. 1982). Hence, H_2 production in all experiments was determined by subtracting the CTR from the TGTR to compare the influence of cultivation conditions on the ratio of produced gasses.

Growth inhibition or limitation of the reference cultivation is visible, as biomass production ceases after 13 h, although 2 g L^{-1} glucose is still present. This observation is likely attributable to pH inhibition because the pH value decreases strongly throughout the cultivation (Fig. 2). Literature shows growth inhibition of *Bacteroides* spp. at pH values below 6 and that growth is stopped completely below pH 5.3 (Flint et al. 2012; Duncan et al. 2009). Besides the low pH, the metabolic activity could be decreased by product inhibition by the organic acids (4.3 g L^{-1}). A product inhibition was shown for *P. vulgatus*-related *B. thetaiotaomicron* (Duncan et al. 2009) and other *Bacteroidetes* strains (Wang et al. 2020) by the acids lactate and acetate. Furthermore, biomass production could be limited by media components apart from glucose.

When biomass and CO_2 production terminates, the acid production continues, leading to the assumption that CO_2 is mainly formed during biomass production. The increased lactate production in the second half of the cultivation may be the easiest way for *P. vulgatus* to balance the production of redox equivalents (van Hoek and Merks 2012). Lactate production is the most straightforward metabolic pathway, requiring only one enzyme—lactate dehydrogenase (Lück and Deppenmeier 2022). The increase of succinate production in the second half of the cultivation may occur because *P. vulgatus* accumulated enough CO_2 for succinate production in the first half (Fischbach and Sonnenburg 2011). Only minimal amounts of CO_2 were released during fermentation, as the bacterium has a profound system for CO_2 fixation with succinate production.

The pH value decreases linearly, corresponding to the linear synthesis of SCFA and *P. vulgatus* converted 77% of carbon from consumed glucose into organic acids. The molar fluxes to CO_2, however, are very low. The carbon balance is closed for this experiment, showing that all gasses and acids contributing carbon to the balance have been successfully evaluated.

To ensure comparability between experiments and account for the difficult handling of anaerobic microorganisms, the offline data of all reference cultivations, including the pH-buffered fermentation, were combined in a box-plot diagram in Fig. 10.

Apart from two outliners in the final OD_{600nm} and final pH, all values are within the 1.5 interquartile range (IQR). In conclusion, the reference cultivations are reliable despite the challenging cultivation of anaerobes and provide valuable insights into the metabolism of *P. vulgatus*.

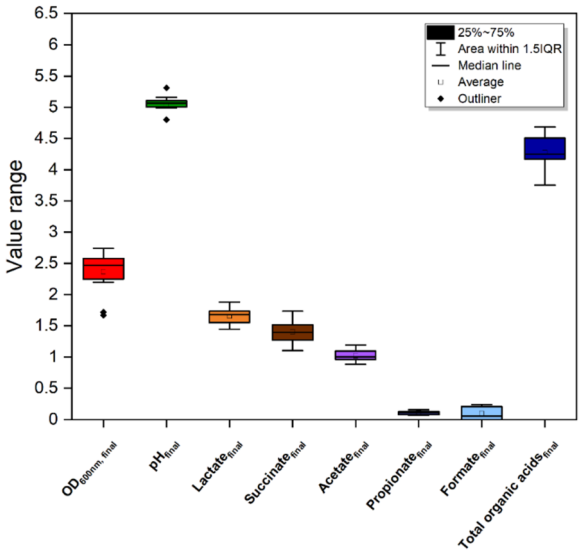

Fig. 10 Box-plot diagram with final offline values of all *P. vulgatus* reference cultivations including the pH-buffered bioreactor cultivation. Medium = DMMG, $c_{Glucose}$ = 6 g L^{-1}, c_{buffer} = 50 mM MOPS, T = 37 °C, $n_{fermenter}$ = 600 rpm, $n_{shake\ flask}$ = 100 rpm, $V_{L,fermenter}$ = 1500 mL, $V_{L,shake\ flask}$ = 50 mL, vvm = 0.2 min^{-1}, gas mix = 1% CO_2 in 99% N_2. The evaluation is based on 11 shake flask cultures and one bioreactor culture

Characterization of cultivation process conditions

After the reference cultivation, process conditions concerning the buffer concentration were investigated. A pH inhibition is observed when 0 mM or only 50 mM MOPS is added (Fig. 3), as the final pH drops below 5.3, resulting in residual glucose (Duncan et al. 2009). Increasing the MOPS concentration to 100 mM leads to full glucose consumption. A further increase to 150 mM results in delayed growth, as an increased osmolality is known to influence the lag phase of microorganisms (Wucherpfennig et al. 2011). The decreasing TGTR and CTR peaks with increasing MOPS concentrations do not correlate with the metabolic activity. More specifically, the acid and biomass production increase with increasing MOPS concentration. The influence of increasing MOPS concentrations is stronger on the CTR than on the TGTR. Therefore, the influence of MOPS seems to be more assertive on CO_2 production than H_2 production. Since the metabolic pathways of *P. vulgatus* are not yet conclusively understood, it is unclear what causes this shift in the CO_2 to H_2 ratio. A pH effect could also cause the difference due to the chemical CO_2/HCO^-_3 balance. CO_2 gasses out of the medium when the pH drops and the pH drop is stronger at lower MOPS concentrations.

The proportions of acids were not affected by MOPS, except for lactate production. The higher the MOPS concentration, the higher the lactate production. The

increased osmotic stress at higher MOPS concentrations can lead to a balancing of redox equivalents most easily via lactate production. Formate production only starts at 50 mM MOPS or higher. In the reference cultivation, formate production took place from 9 h onwards. The shorter cultivation time may not be conducive to formate production. Another reason could be the lower final pH with 0 mM MOPS inhibiting the formate production.

A MOPS concentration of 100 mM is the most suitable for acid and biomass production. However, it led to a longer cultivation time and less gas production, which is why a concentration of 50 mM MOPS was chosen as a good compromise between inhibition by pH and osmolality and the applicability of online measurement.

With increasing osmolality due to NaCl, decreasing gas transfer rate maxima and longer cultivation times were obtained (Fig. 4), similar to the addition of MOPS. However, the decrease is even more pronounced with osmolality than with MOPS. The more pronounced decrease is presumably caused by the positive effect of MOPS buffer on pH being absent, leaving only the negative effect of higher osmolality.

Offline measurements show increasing final pH and OD_{600nm} with increasing NaCl concentrations. The increasing final pH can be explained by the decrease in overall organic acid production with increasing osmolality. Similar to increasing MOPS concentrations, higher NaCl concentrations increase lactate production. Lactate production seems to be a sound strategy for microorganisms under stressful conditions, such as elevated osmolality or low pH. Correspondingly, succinate and acetate production decrease under osmotic stress.

Wetzstein and Gottschalk (1985) showed that for related *B. amylophilus*, increased NaCl concentrations up to 90 mM increased growth. This study used a similar range of 60–90 mM NaCl, and *P. vulgatus* could also profit from increasing Na^+ concentrations (Mulkidjanian et al. 2008; Deusch et al. 2019). On the one hand, inhibition by osmolality is visible. On the other hand, higher NaCl concentrations seem to improve biomass growth. Since acid production is decreased with higher NaCl, more carbon goes into biomass.

Increased initial pH values lead to increased CTRs after 1 h (Fig. 5). An explanation for this might be the pH-dependent chemical CO_2/HCO^-_3 balance. With an elevated, basic pH in the medium (pH of up to 11.0, data not shown), CO_2 remains primarily in solution as HCO^-_3/CO_3^{2-} ions (Tresguerres et al. 2010). With the addition of preculture, which has an acidic pH of 5.0 due to the organic acids that were produced (data not shown), the pH in the medium is strongly decreased. This drop causes the equilibrium to shift towards free CO_2, which gasses out. The increased CO_2 maxima with increased initial pH during cultivation do not correlate with increased metabolic activity regarding OD_{600nm} and acid production. At initial pH values below 7.3, pH inhibition is present as the final pH drops to 5.3 or lower. The trend for the gas transfer rates does not fit in the pH range of 7.29–7.45. These differences are probably because not all pH values could be tested in one experiment, as indicated by different symbols.

The increased osmolality can explain the decreased acid and biomass production at a pH above 7.3. The initial pH had little effect on the organic acid profile, but an optimal pH for growth and acid production is 7.3. The optimal pH corresponds to the natural pH in the gut, as it increases from 6.6 in the small intestine to a mean pH of 7.5 in the terminal ileum (Evans et al. 1988), depending on the exact anatomical site, diet, and microbial fermentation (Duncan et al. 2009).

Influence of initial acid addition

The initial addition of an acid mix with lactate, acetate, and succinate to the DMM-G medium demonstrates inhibition of *P. vulgatus*, compared to the reference (Fig. S8-S10). Experiments with single acid addition show different impacts on the microorganism. An inhibitory effect is confirmed for lactate addition, starting at 1 g L^{-1} lactate and increasing with higher lactate concentrations (Fig. 6). For *Bacteroides thetaiotaomicron*, a concentration greater than 0.9 g L^{-1} lactate was identified as growth-inhibiting (Wang et al. 2020). Increasing lactate concentrations also led to a shift in the H_2/CO_2 production ratio of *P. vulgatus*. Especially for 1.0 g L^{-1} lactate, the lowered CO_2 production is not reflected in the TGTR. As discussed for the reference culture, *P. vulgatus* only produces CO_2 and H_2, which account for the total gas production. Conclusively, lactate addition lowers CO_2 production, while H_2 production is less affected. Besides the observed shift in gas formation, the product ratio shifts from lactate to succinate production due to increased initial lactate addition. Presumably, *P. vulgatus* channels carbon towards other acids once inhibiting lactate concentrations are reached. Acetate, on the other hand, improves glucose utilization, increases acid production, and delays the growth phase (Fig. 7). The delayed growth phase can be explained by the increased osmolality, or acetate itself, as it is as an overflow metabolite mostly considered as inhibiting (Pinhal et al. 2019). It can be suspected that high acetate concentrations inhibit *P. vulgatus* in the first cultivation hours. Still, as glycolytic flux decreases due to the pH drop, acetate becomes beneficial for growth, leading to higher final OD_{600nm} and final acid concentrations. In contrast to the lactate addition experiment, acetate addition does not influence the ratio of produced acids. Interestingly, the same tendency can be seen in the acid mix addition

experiments (Fig. S8-S10), where the product ratio is similar in all cultures, regardless of the amount of added acids. The succinate addition increases growth slightly, compared to the reference (Fig. S6). Succinate is known as a virulence factor in infections containing *Bacteroides* (Rotstein et al. 1987; Rotstein et al. 1985), but also for its role as a beneficial growth factor for rumen bacteria and other gram-negative anaerobes (Lev et al. 1971). For example, Lev et al. (1971) increased the growth rate of the related *Bacteroides melaninogenicus* by succinate addition. They observed that succinate addition functioned as an additional growth factor in the presence of heme and vitamin K. Since vitamin K1 is also present in the DMM-G medium, this could explain the increased growth of *P. vulgatus* by succinate addition. Moreover, succinate as a polyprotic acid with two buffer ranges ($pK_A = 5.62$ and 4.16) could support *P. vulgatus* cultivations by a pH buffering effect. Even though the SCFA succinate and acetate benefit growth and product formation, the mixture of all acids decreases growth, product formation, and gas transfer rates. Presumably, the negative effect of lactate in the acid mix is dominant over the beneficial effect of acetate and succinate.

Scale-up from shake flask to 2 L fermenter and effect of pH control

The progression of OD_{600nm}, pH, and glucose consumption align well between shake flask and fermenter cultivation with the pH-buffered medium in the first 6 h (Fig. 8). The higher OD_{600nm} in the bioreactor confirms that 600 min^{-1} stirring does not exert higher shear stress on the *P. vulgatus* cells, while the culture broth was well mixed. Thus, it can be concluded that the volume-specific gas flow of 0.2 min^{-1} and stirring rate of 600 min^{-1} were chosen adequately for scale-up. The lower initial glucose concentration in the pH-buffered fermenter is one deviation between the two scales. However, as no glucose was added after inoculation, this is likely due to an HPLC inaccuracy of the first sample. The other difference is the addition of antifoam to the fermenter after 6 h cultivation. Antifoams are surface-active agents that favor gas bubble coalescence and reduce the volumetric mass transfer coefficient k_La through changes in the interfacial area a (Al-Masry 1999; Prins and van't Riet 1987). This could decrease the CO_2 availability, which is necessary at a certain level for gut bacteria (Fischbach and Sonnenburg 2011), or change the power input. It is also noticeable that between 6 and 12 h, the OD_{600nm} increases linearly and not exponentially. Because of the faster biomass production in the pH-buffered fermenter, the acid formation (blue stars) is also faster than in the shake flask. For example, the total acid concentration reaches 3 g L^{-1} after 12 h in the shake flask (Fig. 2), while 4 g L^{-1} is obtained at the same time in the pH-buffered fermentation (Fig. 9). However, the final total acid formation is 4.3 g L^{-1} in both scales. Glucose is neither depleted in the shake flask nor in the pH-buffered fermenter. This, and a pH below the optimal range of *P. vulgatus* (Flint et al. 2012; Duncan et al. 2009), confirms the pH-inhibiting effect.

The pH-buffered and pH-controlled cultivations in the 2 L benchtop fermenter are compared to distinguish between pH and organic acids' effects and determine if medium components other than glucose are limiting. The total acid production (blue stars) is shown to be independent of pH buffer or control. Still, biomass growth, glucose conversion, and CO_2 release are higher with pH control set at pH 7.0. This beneficial effect of a pH set point around 7.0 is to be expected since the mean pH in the natural environment of the gut bacterium *P. vulgatus* is in the range of pH 6.0–7.5 (Evans et al. 1988; Fallingborg 1999). A pH control around pH 7.0 by base addition was already successfully applied for axenic cultures or enriched mixed cultures of gut bacteria (Berg et al. 1978; Allison and Macfarlane 1989; Adamberg et al. 2020; Adamberg and Adamberg 2018; Dalland and Hofstad 1974; Isar et al. 2006). Due to glucose depletion after 13 h in the pH-controlled fermentation (vertical, dotted line), a secondary substrate limitation can finally be ruled out for *P. vulgatus* in the DMM-G medium. However, CO_2 production starts to decline in the pH-controlled fermentation already after 9 h, while glucose is still present until 13 h. *P. vulgatus* also stops the production of lactate and formate, producing more acetate and succinate after 9 h in pH-controlled fermentation. Thus, there seems to be a switch in acid formation and corresponding CO_2 release, independently of the pH value. This switch also becomes apparent in the carbon balances. As already discussed for the reference cultivation in Fig. 2, acetate, and biomass production of *P. vulgatus* often correlate with CO_2 release, which matches the data from the pH-controlled fermentation.

Conclusions

Summarizing the experiments, a buffer concentration of 50 mM MOPS and an initial pH of 7.3 benefit *P. vulgatus* shake flask cultivations with 6 g L^{-1} glucose. However, the pH, end products, or a combination of both still inhibit the strain. Very low gas transfer rates were visible, and lactate, succinate, and acetate are the most abundantly produced acids under the tested conditions. An inhibitory effect of lactate on *P. vulgatus* was demonstrated in shake flask experiments. A secondary substrate limitation can be excluded for the applied minimal medium based on stronger growth and glucose depletion in a pH-controlled fermentation.

This work characterizes cultivation process conditions for *P. vulgatus* and explores its fundamental potential as

an SCFA producer. The obtained absolute SCFA values are far from those observed in GMO processes using common industrial producer strains. For example, succinate productivity with *Bacteroides fragilis* in a complex medium was increased to 5.4 g L^{-1} succinate with pH control at 7.0 by Isar et al. (2006). Ultimately, they reached 12.5 g L^{-1} in 30 h with *B. fragilis* by additional control of CO_2 supply and impeller speed (Isar et al. 2006) and mentioned the potential to increase the succinate production even further to 20 g L^{-1} in a theoretical approach (Isar et al. 2007). Therefore, *P. vulgatus* cannot compete with industrial producer strains, as it produces SCFAs like succinate at a maximum of 2.0 g L^{-1} under the used conditions and in axenic culture. However, pH-controlled fermentations could achieve higher succinate titers with *P. vulgatus* in an optimized medium. Another step is applying genetic modifications to enhance the succinate yield and shift acid production from acetate and lactate to succinate. On the fermenter scale, actively controlling CO_2 supply and impeller speed could improve the succinate production, as in Isar et al. 2006 and Isar et al. 2007. The total acid productivity of *P. vulgatus* could also be improved by in-situ product removal during continuous cultivation. Another promising approach to produce bio-based SCFA from organic waste streams, e.g., food waste, are anaerobic mixed culture cultivations. Using renewable substrates will make the production process even more sustainable. This has been shown to be successful by several research groups (Battista et al. 2022; Greses et al. 2022; Pau et al. 2022; Valentino et al. 2021). Further research concerning carbon sources other than glucose, e.g., fructose, xylose, or pectin, as substrates for *P. vulgatus* is currently being conducted. Besides SCFA production, *P. vulgatus* produces bioactive or antimicrobial compounds and can serve as a probiotic (Brinkmann et al. 2022; Wexler 2007; Tan et al. 2019). The potential of *P. vulgatus* to produce the bioactive or antimicrobial compounds and its ability to serve as a probiotic have not been examined in this paper but are interesting approaches for future research. Thus, the characterization of this microorganism concerning SCFA production can benefit future production processes for bioactive or antimicrobial compounds.

Characterizing the key cultivation parameters for *P. vulgatus* in axenic culture and a successful scale-up assesses the potential of *P. vulgatus* for application in biotechnological production processes. As a take-home message, it should be noted that processes with *P. vulgatus* require further cultivation conditions or genetic optimization since *P. vulgatus* cannot compete with established industrial acid producers so far. Nevertheless, the presented results and the application of online measurement techniques contribute to a faster optimization of anaerobic cultivations, paving the way for *P. vulgatus* and related gut microbiota as producers of SCFAs, bioactive or antimicrobial compounds.

Abbreviations

AnaRAMOS	Anaerobic Respiration Activity MOnitoring System
BHI	Brain heart infusion medium
CDW	Cell dry weight
CTR	Carbon dioxide transfer rate
DI water	Deionized water
DMM-G	Defined minimal medium glucose
HPLC	High-performance liquid chromatography
IQR	Interquartile range
k_La	Volumetric mass transfer coefficient
OD_{600nm}	Optical density measured at 600 nm wavelength
PEP	Phosphoenolpyruvate
SCFA	Short-chain fatty acids
STY	Space–time-yield
TGTR	Total gas transfer rate
V_L	Liquid filling volume
Vvm	Volume-specific gas flow

Supplementary Information

The online version contains supplementary material available at https://doi.org/10.1186/s13213-023-01745-4.

Additional file 1: Table S1. Final concentrations of DMM-G medium components used in this work in alphabetical order. The concentrations are based on weighed-in and subsequently completely dissolved amounts before heat-sterilization or filtration. **Table S2.** Parameters and formula for power input calculations of shake flask cultivations. Constants and formula are adapted from Büchs et al. (2000). **Table S3.** Parameters and formula for power input calculations of bioreactor cultivations. **Fig. S1.** Screenshots of slow-motion videos at 400 and 600 rpm in the stirred tank bioreactor. Medium = DMM-G, n = 400 or 600 min^{-1}, V_L = 1500 mL, vvm = 0.2 min^{-1}, gas = N_2. **Fig. S2.** Optical density and cell dry weight correlation. *P. vulgatus*, V_L = 1500 mL, n = 500 rpm, $V_{reactor}$ = 2000 mL, T = 37 °C, DMMG medium w/o bicarbonate, c_{glc} = 6 g/L, pH_{set} of a pH-controlled fermentation = 7.0 (3 M NaOH), vvm = 0.2 min^{-1}, gas mix = 1 % CO_2 and 99 % N_2, N = 3. **Fig. S3.** Effect of changing the initial pH-value on *P. vulgatus* shake flask cultivations**.** Medium = DMMG, $c_{Glucose}$ = 6 g L^{-1}, c_{buffer}= 50 mM MOPS, T = 37 °C, n = 100 rpm, V_L = 50 mL, initial OD = 0.3, different initial pH, vvm = 0.2 min^{-1}, gas mix = 1% CO_2 and 99 % N_2, N = 2, tested initial pH-values: 6.98, 7.07, 7.22, 7.29, 7.33, 7.45, 7.61, 7.73, 7.80, 7.93. Online data of **a** Total gas transfer rate (TGTR) and **b** Carbon dioxide transfer rate (CTR), shadows indicate maximum and minimum values of duplicates. Corresponding to Fig. 5. **Fig. S4.** Carbon balance of *P. vulgatus* cultivations in shake flasks with increasing initial lactate addition. Medium = DMMG, $c_{Glucose}$ = 6 g L^{-1}, c_{buffer} = 50 mM MOPS, T = 37 °C, n = 100 rpm, V_L = 50 mL, initial OD = 0.35, initial pH after inoculation = 7.23, vvm = 0.2 min^{-1}, gas mix = 1 % CO_2 and 99 % N_2, N = 2. **a** Carbon balance in %. The start of the fermentation was set to 100 %. **b** Carbon balance in $mmol_C$ L^{-1}. Corresponding to Fig. 6. **Fig. S5.** Carbon balance of *P. vulgatus* cultivations in shake flasks with increasing initial acetate addition. Medium = DMMG, $c_{Glucose}$ = 6 g L^{-1}, c_{buffer} = 50 mM MOPS, T = 37 °C, n = 100 rpm, V_L = 50 mL, initial OD = 0.40, initial pH after inoculation = 7.20, vvm = 0.2 min^{-1}, gas mix = 1 % CO_2 and 99 % N_2, N = 2. **a** Carbon balance in %. The start of the fermentation was set to 100 %. **b** Carbon balance in $mmol_C$ L^{-1}. Corresponding to Fig. 7. **Fig. S6.** Effect of initial succinate addition to *P. vulgatus* shake flask cultivations. Medium= DMMG, $c_{Glucose}$ = 6 g L^{-1}, c_{buffer} = 50 mM MOPS, T = 37 °C, n = 100 rpm, V_L = 50 mL, initial OD = 0.33, initial pH after inoculation = 6.95, vvm = 0.2 min^{-1}, gas mix = 1 % CO_2 and 99 % N_2, N = 2. Online data of **a** TGTR and **b** CTR. Shadows indicate maximum and minimum values of duplicates. Offline data of **c** produced organic acids including propionate, succinate, acetate and lactate and remaining glucose, **d** initial osmolality, final OD_{600nm} and final pH. Corresponding molar carbon balance in % of the initial carbon can be found in Supplementary Figure S7. **Fig. S7.** Carbon balance of *P. vulgatus* cultivations in shake flasks

with increasing initial succinate addition. Medium = DMMG, $c_{Glucose}$= 6 g L^{-1}, c_{buffer} = 50 mM MOPS, T = 37 °C, n = 100 rpm, V_L = 50 mL, initial OD = 0.33, initial pH after inoculation = 6.95, vvm = 0.2 min^{-1}, gas mix = 1 % CO_2 and 99 % N_2, N = 2. **a** Carbon balance in %. The start of the fermentation was set to 100%. **b** Carbon balance in $mmol_C$ L^{-1}. Corresponding to Fig. S6. **Fig. S8.** Effect of a low initial acid mix addition to *P. vulgatus* shake flask cultivations. Medium= DMMG, $c_{Glucose}$ = 6 g L^{-1}, c_{buffer} = 50 mM MOPS, T = 37 °C, n = 100 rpm, V_L = 50 mL, initial OD = 0.27, initial pH after inoculation = 6.91, vvm = 0.2 min^{-1}, gas mix = 1 % CO_2 and 99 % N_2, N = 2. The ratio of added organic acids was 1.5:1.75:1 for acetate:lactate:succinate. Online data of **a** TGTR and **b** CTR. Shadows indicate maximum and minimum values of duplicates. Offline data of **c** produced organic acids including propionate, succinate, acetate and lactate and remaining glucose, **d** initial osmolality, final OD_{600nm} and final pH. Results of a high initial acid mix can be found in Fig. S9. Corresponding molar carbon balance in % of the initial carbon can be found in Supplementary Figure S10. **Fig. S9.** Effect of a high initial acid mix addition to *P. vulgatus* shake flask cultivations. Medium = DMMG, $c_{Glucose}$ = 6 g L^{-1}, c_{buffer} = 50 mM MOPS, T = 37 °C, n = 100 rpm, V_L= 50 mL, initial OD = 0.21, initial pH after inoculation = 6.94, vvm = 0.2 min^{-1}, gas mix = 1 % CO_2 and 99 % N_2, N = 2. The ratio of added organic acids was 1.5:1.75:1 for acetate:lactate:succinate. Online data of **a** TGTR and **b** CTR. Shadows indicate maximum and minimum values of duplicates. Offline data of **c** produced organic acids including propionate, succinate, acetate and lactate and remaining glucose, **d** initial osmolality, final OD_{600nm} and final pH. Results of a low initial acid mix can be found in Fig. S8. Corresponding molar carbon balance in % of the initial carbon can be found in Supplementary Figure S10. **Fig. S10.** Molar carbon balance of *P. vulgatus* cultivations in shake flasks with increasing initial acid mix addition. Medium = DMMG, $c_{Glucose}$ = 6 g L^{-1}, c_{buffer}= 50 mM MOPS, T = 37 °C, n = 100 rpm, V_L = 50 mL, initial OD* = 0.21, initial pH after inoculation* = 6.94, initial OD** = 0.27, initial pH after inoculation** = 6.91, vvm = 0.2 min^{-1}, gas mix = 1 % CO_2 and 99 % N_2, N = 2. The ratio of added organic acids was 1.5:1.75:1 for acetate:lactate:succinate. Asterisks indicate experiment number one (*) and two (**). **a** Molar carbon balance in % of initial total carbon. Molar carbon from CO_2 was calculated from the CTR integral. **b** Carbon balance in $mmol_C$ L^{-1}. Corresponding to Fig. S8 and Fig. S9. **Fig. S11.** Pressure raw data of the *P. vulgatus* cultivation from Fig. 1 between 6.5 h to 13.5 h. Medium = DMMG, $c_{Glucose}$ = 6 g L^{-1}, c_{buffer} = 50 mM MOPS, T = 37 °C, n = 100 rpm, V_L = 50 mL, initial OD = 0.3, initial pH after inoculation = 7.23, vvm = 0.2 min^{-1}, gas mix = 1% CO_2 and 99% N_2.

Acknowledgements
The authors are grateful to Prof. Dr. Uwe Deppenmeier and Dr. Rebecca Lück (Rhenish Friedrich Wilhelm University of Bonn, DE) for providing the microbial strain used in this work. We thank Maren Großeheide (Chair of Chemical Process Engineering, RWTH Aachen University, Aachen, DE) for gas chromatograph measurements. We are also grateful to René Petri (Chair of Biochemical Engineering, RWTH Aachen University, Aachen, DE) for his invaluable technical support in HPLC analysis.

Authors' contributions
LK, KM, and JB conceived and designed the research. LK, KM, LR, and SY conducted experiments and analyzed data. LK and KM wrote the manuscript. LK, KM, and JB revised the manuscript. All authors read and approved the final manuscript.

Funding
Open Access funding enabled and organized by Projekt DEAL. This study was funded by the German Federal Ministry of Education and Research (BMBF, Grant number 031B0846B). Projekt DEAL, supervised by the German Rectors' Conference, supported publication under Creative Commons license CC-BY.

Availability of data and materials
The datasets used and/or analyzed during the current study are available from the corresponding author upon reasonable request.

Declarations

Ethics approval and consent to participate
Not applicable.

Consent for publication
All authors of the manuscript have read and agreed to its content and are accountable for all aspects of the accuracy and integrity of the manuscript. The article is original, has not already been published in a journal, and is not currently under consideration by another journal.

Competing interests
The authors declare that they have no competing interests.

Received: 24 April 2023 Accepted: 18 December 2023
Published online: 26 January 2024

References

Adamberg K, Adamberg S (2018) Selection of fast and slow growing bacteria from fecal microbiota using continuous culture with changing dilution rate. Microb Ecol Health Dis 29(1):1549922. https://doi.org/10.1080/16512235.2018.1549922

Adamberg K, Valgepea K, Vilu R (2015) Advanced continuous cultivation methods for systems microbiology. Microbiology 161(9):1707–1719. https://doi.org/10.1099/mic.0.000146

Adamberg K, Raba G, Adamberg S (2020) Use of changestat for growth rate studies of gut microbiota. Front Bioeng Biotechnol 8:24. https://doi.org/10.3389/fbioe.2020.00024

Allison C, Macfarlane GT (1989) Influence of pH, nutrient availability, and growth rate on amine production by *Bacteroides fragilis* and *Clostridium perfringens*. Appl Environ Microbiol 55(11):2894–2898. https://doi.org/10.1128/aem.55.11.2894-2898.1989

Al-Masry WA (1999) Effects of antifoam and scale-up on operation of bioreactors. Chem Eng Process 38(3):197–201. https://doi.org/10.1016/S0255-2701(99)00014-8

Anderlei T, Büchs J (2001) Device for sterile online measurement of the oxygen transfer rate in shaking flasks. Biochem Eng J 7(2):157–162. https://doi.org/10.1016/S1369-703X(00)00116-9

Anderlei T, Zang W, Papaspyrou M, Büchs J (2004) Online respiration activity measurement (OTR, CTR, RQ) in shake flasks. Biochem Eng J 17(3):187–194. https://doi.org/10.1016/S1369-703X(03)00181-5

Battista F, Strazzera G, Valentino F, Gottardo M, Villano M, Matos M, Silva F, M. Reis M, Mata-Alvarez J, Astals S, Dosta J, Jones R J, Massanet-Nicolau J, Guwy A, Pavan P, Bolzonella D, Majone M (2022) New insights in food waste, sewage sludge and green waste anaerobic fermentation for short-chain volatile fatty acids production: A review. J Environ Chem Eng 10. 5:108319 https://doi.org/10.1016/j.jece.2022.108319

Berg JO, Nord CE, Wadström T (1978) Formation of glycosidases in batch and continuous culture of *Bacteroides fragilis*. Appl Environ Microbiol 35(2):269–273. https://doi.org/10.1128/AEM.35.2.269-273.1978

Bredwell MD, Srivastava P, Worden RM (1999) Reactor design issues for synthesis-gas fermentations. Biotechnol Prog 15(5):834–844. https://doi.org/10.1021/bp990108m

Brinkmann S, Spohn MS, Schäberle TF (2022) Bioactive natural products from *Bacteroidetes*. Nat Prod Rep 39(5):1045–1065. https://doi.org/10.1039/d1np00072a

Büchs J, Maier U, Milbradt C, Zoels B (2000) Power consumption in shaking flasks on rotary shaking machines: I. Power consumption measurement in unbaffled flasks at low liquid viscosity. Biotechnol Bioeng 68(6):589–593. https://doi.org/10.1002/(sici)1097-0290(20000620)68:6<589::aid-bit1>3.0.co;2-j

Bulushev DA, Ross JRH (2018) Towards sustainable production of formic acid. Chem Sus Chem 11(5):821–836. https://doi.org/10.1002/cssc.201702075

Cato E P, Johnson J L (1976) Reinstatement of species rank for *Bacteroides fragilis, B. ovatus, B. distasonis, B. thetaiotaomicron*, and *B. vulgatus*: designation of neotype strains for *Bacteroides fragilis* (Veillon and Zuber) Castellani and Chalmers and *Bacteroides thetaiotaomicron* (Distaso) Castellani and

Chalmers. Int J Syst Bacteriol 26. 2:230–237. https://doi.org/10.1099/00207713-26-2-230.
Chung WSF, Meijerink M, Zeuner B, Holck J, Louis P, Meyer AS, Wells JM, Flint HJ, Duncan SH (2017) Prebiotic potential of pectin and pectic oligosaccharides to promote anti-inflammatory commensal bacteria in the human colon. FEMS Microbiol Ecol 93:11. https://doi.org/10.1093/femsec/fix127
Cummings JH, Macfarlane GT (1991) The control and consequences of bacterial fermentation in the human colon. J Appl Bacteriol 70(6):443–459. https://doi.org/10.1111/j.1365-2672.1991.tb02739.x
Cummings JH, Pomare EW, Branch WJ, Naylor CP, Macfarlane GT (1987) Short chain fatty acids in human large intestine, portal, hepatic and venous blood. Gut 28(10):1221–1227. https://doi.org/10.1136/gut.28.10.1221
Dalland E, Hofstad T (1974) Growth of *Bacteroides fragilis* in continuous culture and in batch cultures at controlled pH. Appl Microbiol 28(5):856–860. https://doi.org/10.1128/am.28.5.856-860.1974
de Vos WM, Tilg H, van Hul M, Cani PD (2022) Gut microbiome and health: mechanistic insights. Gut 71(5):1020–1032. https://doi.org/10.1136/gutjnl-2021-326789
Deusch S, Bok E, Schleicher L, Seifert J, Steuber J (2019) Occurrence and function of the Na^+-translocating NADH:quinone oxidoreductase in *Prevotella spp*. Microorganisms 7:5. https://doi.org/10.3390/microorganisms7050117
Duncan SH, Louis P, Thomson JM, Flint HJ (2009) The role of pH in determining the species composition of the human colonic microbiota. Environ Microbiol 11(8):2112–2122. https://doi.org/10.1111/j.1462-2920.2009.01931.x
Evans DF, Pye G, Bramley R, Clark AG, Dyson TJ, Hardcastle JD (1988) Measurement of gastrointestinal pH profiles in normal ambulant human subjects. Gut 29(8):1035–1041. https://doi.org/10.1136/gut.29.8.1035
Fallingborg J (1999) Intraluminal pH of the human gastrointestinal tract. Dan Med Bull 46(3):183–196
Fischbach MA, Sonnenburg JL (2011) Eating for two: how metabolism establishes interspecies interactions in the gut. Cell Host Microbe 10(4):336–347. https://doi.org/10.1016/j.chom.2011.10.002
Flint HJ, Scott KP, Louis P, Duncan SH (2012) The role of the gut microbiota in nutrition and health. Nat Rev Gastroenterol Hepatol 9(10):577–589. https://doi.org/10.1038/nrgastro.2012.156
Franke T (2020) Aufklärung des zentralen Kohlenstoff- und Energiemetabolismus des Darmbakteriums *Prevotella copri*. Dissertation 109(4):528–540. https://doi.org/10.1111/mmi.14058
Franke T, Deppenmeier U (2018) Physiology and central carbon metabolism of the gut bacterium *Prevotella copri*. In: Molecular microbiology 109(4):S. 528–540. https://doi.org/10.1111/mmi.14058
García-López M, Meier-Kolthoff JP, Tindall BJ, Gronow S, Woyke T, Kyrpides NC, Hahnke RL, Göker M (2019) Analysis of 1,000 type-strain genomes improves taxonomic classification of *Bacteroidetes*. Front Microbiol 10:2083. https://doi.org/10.3389/fmicb.2019.02083
Greses S, Tomás-Pejó E, González-Fernández C (2022) Food waste valorization into bioenergy and bioproducts through a cascade combination of bioprocesses using anaerobic open mixed cultures. J Clean Prod 372:133680. https://doi.org/10.1016/j.jclepro.2022.133680
van Hoek M J A, Merks R M H (2012) Redox balance is key to explaining full vs. partial switching to low-yield metabolism. BMC Syst Biol. 6:22. https://doi.org/10.1186/1752-0509-6-22.
Isar J, Agarwal L, Saran S, Saxena RK (2006) Succinic acid production from *Bacteroides fragilis*: process optimization and scale up in a bioreactor. Anaerobe 12(5–6):231–237. https://doi.org/10.1016/j.anaerobe.2006.07.001
Isar J, Agarwal L, Saran S, Kaushik R, Saxena RK (2007) A statistical approach to study the interactive effects of process parameters on succinic acid production from *Bacteroides fragilis*. Anaerobe 13(2):50–56. https://doi.org/10.1016/j.anaerobe.2006.12.002
Kattel A, Morell I, Aro V, Lahtvee P-J, Vilu R, Jõers A, Nahku R (2023) Detailed analysis of metabolism reveals growth-rate-promoting interactions between *Anaerostipes caccae* and *Bacteroides* spp. Anaerobe 79:102680. https://doi.org/10.1016/j.anaerobe.2022.102680
Kazimierowicz J, Dębowski M, Zieliński M (2022) Effectiveness of hydrogen production by *Bacteroides vulgatus* in psychrophilic fermentation of cattle slurry. Clean Technol 4(3):806–814. https://doi.org/10.3390/cleantechnol4030049
Koblitz J, Halama P, Spring S, Thiel V, Baschien C, Hahnke RL, Pester M, Overmann J, Reimer LC (2023) MediaDive: the expert-curated cultivation media database. Nucleic Acids Res 51(D1):D1531–D1538. https://doi.org/10.1093/nar/gkac803
Koh A, de Vadder F, Kovatcheva-Datchary P, Bäckhed F (2016) From dietary fiber to host physiology: short-chain fatty acids as key bacterial metabolites. Cell 165(6):1332–1345. https://doi.org/10.1016/j.cell.2016.05.041
Lim HG, Lee JH, Noh MH, Jung GY (2018) Rediscovering acetate metabolism: Its potential sources and utilization for biobased transformation into value-added chemicals. J Agric Food Chem 66(16):3998–4006. https://doi.org/10.1021/acs.jafc.8b00458
Louis P, Flint HJ (2017) Formation of propionate and butyrate by the human colonic microbiota. Environ Microbiol 19(1):29–41. https://doi.org/10.1111/1462-2920.13589
Lück R, Deppenmeier U (2022) Genetic tools for the redirection of the central carbon flow towards the production of lactate in the human gut bacterium *Phocaeicola (Bacteroides) vulgatus*. Appl Microbiol Biotechnol 106(3):1211–1225. https://doi.org/10.1007/s00253-022-11777-6
Macfarlane S, Macfarlane GT (2003) Regulation of short-chain fatty acid production. Proc Nutr Soc 62(1):67–72. https://doi.org/10.1079/PNS2002207
Macy JM, Probst I (1979) The Biology of Gastrointestinal *Bacteroides*. Annu Rev Microbiol 33:561–594. https://doi.org/10.1146/annurev.mi.33.100179.003021
Mayhew JW, Onderdonk AB, Gorbach SL (1975) Effects of time and growth media on short-chain fatty acid production by *Bacteroides fragilis*. Applied Microbiol 29(4):472–475. https://doi.org/10.1128/am.29.4.472-475.1975
McCarthy RE, Pajeau M, Salyers AA (1988) Role of starch as a substrate for *Bacteroides vulgatus* growing in the human colon. Appl Environ Microbiol 54(8):1911–1916. https://doi.org/10.1128/AEM.54.8.1911-1916.1988
McKay LF, Holbrook WP, Eastwood MA (1982) Methane and hydrogen production by human intestinal anaerobic bacteria. Acta Pathol Microbiol Immunol Scand B 90(3):257–260. https://doi.org/10.1111/j.1699-0463.1982.tb00114.x
Miebach K, Finger M, Scherer AMK, Maaß CA, Büchs J (2023) Hydrogen online monitoring based on thermal conductivity for anaerobic microorganisms. Biotechnol Bioeng 120(8):2199–2213. https://doi.org/10.1002/bit.28502
Mulkidjanian AY, Dibrov P, Galperin MY (2008) The past and present of sodium energetics: may the sodium-motive force be with you. Biochim Biophys Acta 1777(7–8):985–992. https://doi.org/10.1016/j.bbabio.2008.04.028
Munch G, Schulte A, Mann M, Dinger R, Regestein L, Rehmann L, Büchs J (2020) Online measurement of CO_2 and total gas production in parallel anaerobic shake flask cultivations. Biochem Eng J 153:107418. https://doi.org/10.1016/j.bej.2019.107418
Neff A, Lück R, Hövels M, Deppenmeier U (2023) Expanding the repertoire of counterselection markers for markerless gene deletion in the human gut bacterium *Phocaeicola vulgatus*. Anaerobe 81:102742. https://doi.org/10.1016/j.anaerobe.2023.102742
Onderdonk AB, Cisneros RL, Bronson RT (1983) Enhancement of experimental ulcerative colitis by immunization with *Bacteroides vulgatus*. Infect Immun 42(2):783–788. https://doi.org/10.1128/iai.42.2.783-788.1983
Pau S, Tan LC, Lens PNL (2022) Effect of pH on lactic acid fermentation of food waste using different mixed culture inocula. J Chem Technol Biotechnol 97(4):950–961. https://doi.org/10.1002/jctb.6982
Pinhal S, Ropers D, Geiselmann J, de Jong H (2019) Acetate metabolism and the inhibition of bacterial growth by acetate. J Bacteriol 201:13. https://doi.org/10.1128/JB.00147-19
Prins A, van't Riet K, (1987) Proteins and surface effects in fermentation: foam, antifoam and mass transfer. Trends Biotechnol 5(11):296–301. https://doi.org/10.1016/0167-7799(87)90080-1
Reilly S (1980) The carbon dioxide requirements of anaerobic bacteria. J Med Microbiol 13(4):573–579. https://doi.org/10.1099/00222615-13-4-573
Ríos-Covián D, Ruas-Madiedo P, Margolles A, Gueimonde M, los Reyes-Gavilán C G de, Salazar N (2016) Intestinal short chain fatty acids and their link with diet and human health. Front Microbiol 7:185https://doi.org/10.3389/fmicb.2016.00185
Salyers AA (1984) *Bacteroides* of the human lower intestinal tract. Annu Rev Microbiol 38:293–313. https://doi.org/10.1146/annurev.mi.38.100184.001453
Savage DC (1977) Microbial ecology of the gastrointestinal tract. Annu Rev Microbiol 31:107–133. https://doi.org/10.1146/annurev.mi.31.100177.000543

Sonnenburg ED, Zheng H, Joglekar P, Higginbottom SK, Firbank SJ, Bolam DN, Sonnenburg J (2010) Specificity of polysaccharide use in intestinal *Bacteroides* species determines diet-induced microbiota alterations. Cell 141(7):1241–1252. https://doi.org/10.1016/j.cell.2010.05.005

Takors R, Kopf M, Mampel J, Bluemke W, Blombach B, Eikmanns B, Bengelsdorf FR, Weuster-Botz D, Dürre P (2018) Using gas mixtures of CO, CO_2 and H_2 as microbial substrates: the do's and don'ts of successful technology transfer from laboratory to production scale. Microb Biotechnol 11(4):606–625. https://doi.org/10.1111/1751-7915.13270

Tan H, Zhai Q, Chen W (2019) Investigations of *Bacteroides spp.* towards next-generation probiotics. Food Res Int 116:637–644. https://doi.org/10.1016/j.foodres.2018.08.088

Traore SI, Khelaifia S, Armstrong N, Lagier JC, Raoult D (2019) Isolation and culture of *Methanobrevibacter smithii* by co-culture with hydrogen-producing bacteria on agar plates. Clin Microbiol Infect 25(12):1561.e1-1561.e5. https://doi.org/10.1016/j.cmi.2019.04.008

Tresguerres M, Buck J, Levin LR (2010) Physiological carbon dioxide, bicarbonate, and pH sensing. Pflugers Arch 460(6):953–964. https://doi.org/10.1007/s00424-010-0865-6

Valentino F, Munarin G, Biasiolo M, Cavinato C, Bolzonella D, Pavan P (2021) Enhancing volatile fatty acids (VFA) production from food waste in a two-phases pilot-scale anaerobic digestion process. J Environ Chem Eng 9(5):106062. https://doi.org/10.1016/j.jece.2021.106062

Varel V H, Bryant M P (1974) Nutritional features of *Bacteroides fragilis* subsp. *fragilis*. Appl Microbiol 28. 2:251–257. https://doi.org/10.1128/am.28.2.251-257.1974.

Wang X, Li Y, Zhang Y, Pan Y-R, Li L, Liu J, Butler D (2019) Stepwise pH control to promote synergy of chemical and biological processes for augmenting short-chain fatty acid production from anaerobic sludge fermentation. Water Res 155:193–203. https://doi.org/10.1016/j.watres.2019.02.032

Wang S P, Rubio L A, Duncan S H, Donachie G E, Holtrop G, Lo G, Farquharson F M, Wagner J, Parkhill J, Louis P, Walker A W, Flint H J (2020) Pivotal roles for pH, lactate, and lactate-utilizing bacteria in the stability of a human colonic microbial ecosystem. mSystems 5. 5. https://doi.org/10.1128/mSystems.00645-20.

Wetzstein HG, Gottschalk G (1985) A sodium-stimulated membrane-bound fumarate reductase system in *Bacteroides amylophilus*. Arch Microbiol 143(2):157–162. https://doi.org/10.1007/BF00411041

Wexler HM (2007) *Bacteroides*: the good, the bad, and the nitty-gritty. Clin Microbiol Rev 20(4):593–621. https://doi.org/10.1128/CMR.00008-07

Wilson AS, Koller KR, Ramaboli MC, Nesengani LT, Ocvirk S, Chen C, Flanagan CA, Sapp FR, Merritt ZT, Bhatti F, Thomas TK, O'Keefe SJD (2020) Diet and the human gut microbiome: an international review. Dig Dis Sci 65(3):723–740. https://doi.org/10.1007/s10620-020-06112-w

Wolin MJ (1969) Volatile fatty acids and the inhibition of *Escherichia coli* growth by rumen fluid. Appl Microbiol 17(1):83–87. https://doi.org/10.1128/am.17.1.83-87.1969

Wucherpfennig T, Hestler T, Krull R (2011) Morphology engineering–osmolality and its effect on Aspergillus niger morphology and productivity. Microb Cell Fact 10:58. https://doi.org/10.1186/1475-2859-10-58

Publisher's Note